



134
965
THS

1
2010

LIBRARY
Michigan State
University

This is to certify that the
thesis entitled

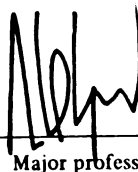
**FICTITIOUS DOMAIN SOLUTION OF FREQUENCY RESPONSE
PROBLEMS**

presented by

Sudarsanam Chellappa

has been accepted towards fulfillment
of the requirements for

MS Mechanical Engineering
_____ degree in _____



Major professor

Date 6 JULY, 2000

PLACE IN RETURN BOX to remove this checkout from your record.
TO AVOID FINES return on or before date due.
MAY BE RECALLED with earlier due date if requested.

DATE DUE	DATE DUE	DATE DUE

FICTITIOUS DOMAIN SOLUTION OF FREQUENCY RESPONSE PROBLEMS

By

Sudarsanam Chellappa

A THESIS

Submitted to
Michigan State University
In partial fulfillment of the requirements
For the degree of

MASTER OF SCIENCE

Department of Mechanical Engineering

2000

ABSTRACT

FICTITIOUS DOMAIN SOLUTION OF FREQUENCY RESPONSE PROBLEMS.

by

Sudarsanam Chellappa

An alternative solution strategy for frequency response problems in elasticity is proposed. This strategy uses a mesh-less finite element method, derived in a periodic domain setting, extended to allow the analysis of arbitrary geometries with the use of a fictitious domain. This solution technique is designed to solve problems with a large number of degrees of freedom and it requires the use of iterative solvers where preconditioning is necessary for reasonable convergence rates. A preconditioned conjugate gradient-type solver is used with a preconditioner specially designed for this problem so that the convergence of the iterative algorithm is quick and insensitive to the size of the problem. Some examples illustrating this approach are provided.

To my parents

ACKNOWLEDGEMENTS

I would like to thank my advisor Dr. Alejandro Diaz. Your guidance and support has been invaluable. I would also like to thank the members of my committee: Dr. Andre Benard and Dr. Alan Haddow. Thank you for the time spent in reviewing this document and providing valuable suggestions.

TABLE OF CONTENTS

LIST OF FIGURES.....	vii
-----------------------------	------------

Chapter 1

Introduction	1
---------------------------	----------

Chapter 2

Fictitious Domain Approach.....	7
2.1 Introduction.....	7
2.2 Field Equations of Elastostatics.....	8
2.3 Problem Statement	9
2.4 Summary	12

Chapter 3

Applying Fictitious Domain Methods To Solve Frequency Response

Problems in Two Dimensions.....	14
3.1 Introduction.....	14
3.2 Field Equations in Elastodynamics.....	15
3.3 Problem Statement	16
3.4 Problem Discretization	18
3.5 Solution Strategy	20
3.6 Preconditioning	21
3.7 Derivation of the Preconditioner	22
3.8 Inversion of the Preconditioner	24
3.9 Examples.....	26
3.9.1 Example 1.....	26
3.9.2 Example 2.....	33
3.9.3 Example 3.....	36
3.9.4 Example 4.....	39

Chapter 4

Solving Frequency Response Problems in Three Dimensions.....	42
4.1 Introduction.....	42
4.2 Problem Statement	42
4.3 Problem Discretization in Three Dimensions	44
4.4 Solution Strategy	46
4.5 Derivation of the Preconditioner	47
4.6 Examples	51
4.6.1 Example 1.....	51
4.6.2 Example 2.....	54

Chapter 5	
Conclusions	57
APPENDIX	59
BIBLIOGRAPHY	61

List of Figures

2.1 Original Problem on Ω_2	9
2.2 Fictitious Domain Problem	10
2.3 Ω -Periodic domain	11
2.4 A circular domain at various resolutions	13
3.1 Frequency response problem on an arbitrary domain	16
3.2 Frequency response problem on Ω	17
3.3 Structure of block-circulant matrices	23
3.4 Cantilever beam with a tip load	26
3.5 Comparison of fictitious domain solution with exact result	27
3.6 Performance of the solver for various preconditioners	28
3.7 Performance of the solver for different frequencies and resolutions	30
3.8 Frequency response plots	32
3.9 One quarter of a plate with a center hole	33
3.10 Performance of the solver for different frequencies and resolutions	34
3.11 Frequency response plot	35
3.12 A curved beam, fixed at one end and a tip load at the other	36
3.13 Performance of the solver for different frequencies and resolutions	37
3.14 Frequency response plot	38
3.15 An arbitrary geometry fixed at two ends and a force in the middle	39
3.16 Performance of the solver for different frequencies and resolutions	40
3.17 Frequency response plot	41
4.1 Example of a voxel discretization.	44
4.2 Constrained and fictitious degrees of freedom	47
4.3 Structure of two-block circulant matrices	48
4.4 A rectangular bar with a tip load	51
4.5 Performance of the solver for different frequencies and resolutions	52
4.6 Frequency response plots	53
4.7 One half of a crankshaft, constrained along its length	54
4.8 Performance of the solver for different frequencies and resolutions	55
4.9 Frequency response plot	56

Chapter 1

Introduction

The goal of solving frequency response problems is to determine the response of a structure subject to a periodic forcing. This is of interest in design problems in which the mechanical and structural systems are subjected to harmonically varying external loads caused by reciprocating power train or other rotating machinery such as motors, fans, compressors and forging hammers. When a machine or any structure oscillates in some form of periodic or random motion, the motion generates alternating pressure waves that propagate from the moving surface at the velocity of sound. These motions with frequencies in the audible range can cause discomfort to the people nearby. For instance, in an automobile the input forces transmitted from the road and the power train excite the vehicle compartment boundary panels. Airplane body and wing structures are also subjected to a harmonic

load transmitted from the propulsion system causing noise problem, cracks, fatigue failure of the tail shaft and discomfort to the crew. This provides a motivation for us to study the frequency response of a structure.

The equations associated with this problem are the partial differential equations associated with linear elasticity. Typically, these problems are solved using the finite element method. In this approach, the problem domain is discretized into small elements and the local response is approximated using polynomial shape functions associated with a particular choice of a finite element. This results in discretized set of linear equations of the form $\mathbf{Ax} = \mathbf{b}$, where \mathbf{A} is the coefficient matrix resulting from the finite element discretization, \mathbf{b} is the force vector and \mathbf{x} is the response. Typically, a solution to the above set of linear equations is obtained by inverting the coefficient matrix (\mathbf{A}) using some standard techniques like LU-decomposition. These techniques however require that the matrix be stored *in core*. There are difficulties, however, that arise when the size of the problem is very large as in the case when a very fine resolution of the geometry or the material distribution is necessary. As the problem size increases, the memory requirements and CPU time necessary to obtain finite element solutions dominate the overall process. For large-scale problems, high computational demands often make the problems impractical to solve using reasonable computational resources.

In very large problems one must resort to iterative procedures that do not require storage of the coefficient matrix. Iterative solvers need more CPU time than direct methods but use substantially less in-core memory. Now, the rate of convergence becomes an important issue. It is well known that when the standard finite element approach is used, the rate of convergence of iterative schemes such as *preconditioned conjugate gradient methods* decays as the resolution increases, eventually rendering the approach useless [1]. This motivates the search for a solution scheme that is better suited for these kinds of large-scale problems. This dissertation presents a new method to solve large-scale frequency response problems by modifying the standard finite element approach using *mesh-less* techniques that are specially tailored to solve these problems.

Our goal is to develop a new analysis technique to determine approximate solutions to the elasticity equations associated with the frequency response problem. We seek an analysis technique that performs analysis at rates that are independent of resolution. To meet this goal we turn to the *fictitious domain technique*.

Our approach is based on *mesh-less* methods for analysis that accurately predicts the elastic response of highly detailed mechanical components. The discretization is developed from an image of the component embedded into a

simple fictitious domain: a square in two dimensions and a cube in three dimensions. The fictitious domain is used to simplify the analysis by embedding the originally complex geometry of the structure in a simple regular domain. In two dimensions, this process corresponds to a *pixel* level discretization of the component, while in three dimensions the discretization is similar to a *voxel* discretization (the three-dimensional equivalent to *pixels*). Due to potentially high resolution of the image discretization for reasons of accuracy, an iterative preconditioned conjugate gradient type solver is incorporated to solve the resulting linear equations. A special preconditioner that results in convergence rates that are insensitive to the resolution of the image discretization is used. Each *pixel* or *voxel* in the image discretization is associated with a single finite element, thus avoiding the time consuming *meshing* process often required for standard finite element techniques. One important property of this numerical scheme is that the coding for the solution of the boundary value problem is *independent* of the geometry of the boundary. Normally in finite element approaches to such a boundary value problem, one has a finite element grid, which is *adapted* to the boundary. This is not necessary for this scheme, which gives it great flexibility in applications.

These *mesh-less* techniques have been used effectively by DeRose and Diaz for solving topology optimization problems in *elastostatics* using a wavelet-

Galerkin approach [2,3,4]. In this approach, bases constructed from refinable shift-invariant wavelets were combined with traditional Galerkin techniques to perform the required analysis in the generalized topology optimization problems. The boundary conditions were implemented in the form of Lagrange multipliers. This resulted in a discretized set of linear equations whose coefficient matrix is real, symmetric and positive semi-definite. They solved this with a Preconditioned Conjugate Gradient solver by incorporating a preconditioner based on the work of Bramble and Pasciak [5].

Earlier work on the solution of partial differential equations using fictitious domain techniques has been mainly due to R.O. Wells, X. Zhou, R. Glowinski, T.W. Pan, et al, some of which are discussed briefly here. In 1993, Wells and Zhou [6] published a modified form of the classical penalty method for solving a Dirichlet boundary value problem using wavelets. This was based on the fact that one could expand the boundary measure under the chosen basis, which led to a fast, approximate calculation of boundary integrals. Glowinski et al in 1995 [7] presented a new fictitious domain formulation for the strongly elliptic boundary value problem with Neumann boundary conditions for a bounded domain in a finite-dimensional Euclidean space with a smooth boundary and extended that to a larger rectangular domain with periodic boundary conditions. They have presented the application of this method using both wavelet-Galerkin and finite element approximation schemes. They have also shown that the convergence rates of both schemes are comparable.

In 1996, Glowinski et al [8] presented a wavelet multigrid preconditioner for the conjugate gradient method that acted as an efficient solver for the linear system arising from a wavelet-Galerkin discretization of a Dirichlet boundary value problem via a penalty/fictitious domain formulation. They have also described some numerical experiments to confirm the efficiency of the iterative solver.

The remainder of the dissertation is organized as follows. Chapter 2 discusses the fundamentals of the fictitious domain approach using a simple elastostatic case for better understanding. Chapter 3 discusses the application of the fictitious domain approach to solve frequency response problems in two dimensions. Chapter 4 talks about solving three-dimensional frequency response problems and describes a slightly modified version of the solution technique used in the case of two-dimensional problems. Conclusions about this method are provided in Chapter 5.

Chapter 2

Fictitious Domain Approach

2.1 Introduction

This chapter discusses the basics of the fictitious domain approach and its application to solve problems in linear elasticity. The goal of the fictitious domain approach is to solve problems with arbitrary domains by embedding them into a simple domain, a square in two dimensions or a cube in three dimensions, and solving instead an equivalent problem in the simplified geometry. Hopefully, recasting the problem in the simplified domain facilitates the use of efficient solution techniques without compromising the accuracy in the domain of interest.

The following sections discuss this approach. We have shown its application to solve the simple static elasticity problems so as to facilitate better understanding of the approach. For a more complete discussion of the fictitious domain approach see the work of Wells, Glowinski et al [6,7,8].

2.2 Field Equations of Elastostatics

- **Equilibrium Equations:**

$$\sigma_{ji,j} + f_i = 0 \quad (2.1)$$

- **Strain-Displacement relationship:**

$$\varepsilon_{ij} = \frac{1}{2}(u_{i,j} + u_{j,i}) \quad (2.2)$$

- **Stress-Strain relationship:**

$$\sigma_{ij} = D_{ijkl} \varepsilon_{kl} \quad (2.3)$$

Here, σ is the elastic stress tensor, ε is the elastic strain tensor, \mathbf{f} is the body force per unit volume, \mathbf{u} is the displacement field and \mathbf{D} is the elastic material tensor.

Combining the above three equations we get

$$D_{ijkl} u_{i,jk} + f_i = 0 \quad (2.4)$$

Multiplying this equation with a weight function (\mathbf{w}) and integrating over the volume we get it into the familiar weak form, which is

$$\int_V \mathbf{D} \varepsilon(\mathbf{u}) \varepsilon(\mathbf{w}) dV = \int_V \mathbf{f}^T \mathbf{w} dV \quad \text{for all } \mathbf{w}_i \in H^1(V) \quad (2.5)$$

Here $H^k(V)$ denotes the Sobolev space of L^2 functions in V whose k^{th} derivative is also in $L^2(V)$. L^2 is the set of functions $f: \mathbb{R} \rightarrow \mathbb{R}$ such that the integral of f^2 in V is finite, i.e.,

$$f \in L^2(V) \Leftrightarrow \int_V f^2 dV < \infty \quad (2.6)$$

2.3 Problem Statement

We consider a two-dimensional elasticity problem on an arbitrary domain Ω_2 , with displacement boundary conditions specified on Γ , a subset of $\partial\Omega_2$, as shown in Figure 2.1.

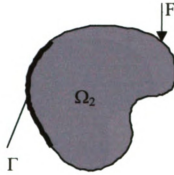


Figure 2.1 Original problem on Ω_2

The above problem can be expressed as

Find $v_i \in V_{\Omega_2}$ such that

$$\int_{\Omega_2} \mathbf{D}_{\Omega_2} \varepsilon(\mathbf{v}) \varepsilon(\mathbf{w}) d\Omega = L_{\Omega_2}(\mathbf{w}) \quad \text{for all } w_i \in V_{\Omega_2} \quad (2.7)$$

where

$$L_{\Omega_2}(\mathbf{w}) = \int_{\Omega_2} \mathbf{f}^T \mathbf{w} d\Omega \quad (2.8)$$

and

$$w_i \in V_{\Omega_2} \equiv \left\{ w_i \in H^1(\Omega_2) : w_i = 0 \text{ in } \Gamma \subseteq \partial\Omega_2 \right\} \quad (2.9)$$

Note that $\mathbf{v} = (v_x, v_y)$, $\mathbf{f} = (f_x, f_y)$ and $\mathbf{D}_{\Omega_2} = \mathbf{D}_{\Omega_2}(x, y)$.

Now we embed Ω_2 into a regular (fictitious) domain Ω_1 to get a new heterogeneous domain $\Omega (= [0, d] \times [0, d]) = \Omega_1 \cup \Omega_2$ with $\Omega_1 \cap \Omega_2 = \emptyset$ as shown in Figure 2.2 and introduce another constraint, such that the solution is Ω -periodic.

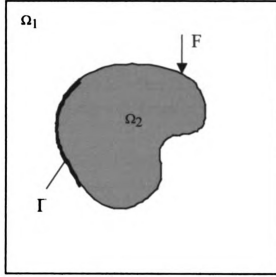


Figure 2.2. Fictitious domain problem

The problem statement can be rewritten as

$$\begin{aligned} &\text{Find } u_i \in K_\Omega \text{ such that} \\ &\int_{\Omega} \mathbf{D}_\Omega \varepsilon(\mathbf{u}) \varepsilon(\mathbf{w}) d\Omega = \int_{\Omega} \mathbf{f}^T \mathbf{w} d\Omega \quad \text{for all } \mathbf{w}_i \in K_\Omega \end{aligned} \quad (2.10)$$

where

$$K_\Omega \equiv \{u_i \in V_\Omega : u_i = 0 \text{ in } \Gamma \subseteq \partial\Omega_2\} \quad (2.11)$$

and

$$V_\Omega \equiv \{u_i \in H^1(\Omega) : u_i \text{ is } \Omega\text{-periodic}\} \quad (2.12)$$

Now, this problem looks exactly like a problem produced by the homogenization procedure for computing the homogenized coefficients of composites of essentially different components with a periodic structure. The Ω -periodicity is introduced so as to facilitate a particular solution technique (to be discussed at a later stage) specially tailored to such kind of problems. The meaning of Ω -periodicity can be mathematically stated as shown in (2.13) and illustrated in Figure 2.3.

$$\begin{aligned} \text{A function } v : \Omega \rightarrow \mathbb{R}, \text{ where } \Omega \text{ is } [0, d] \times [0, d], \text{ is } \Omega\text{-periodic, if} \\ v(x, y) = v(x + d, y + d) \text{ for all } (x, y) \in \Omega \end{aligned} \quad (2.13)$$

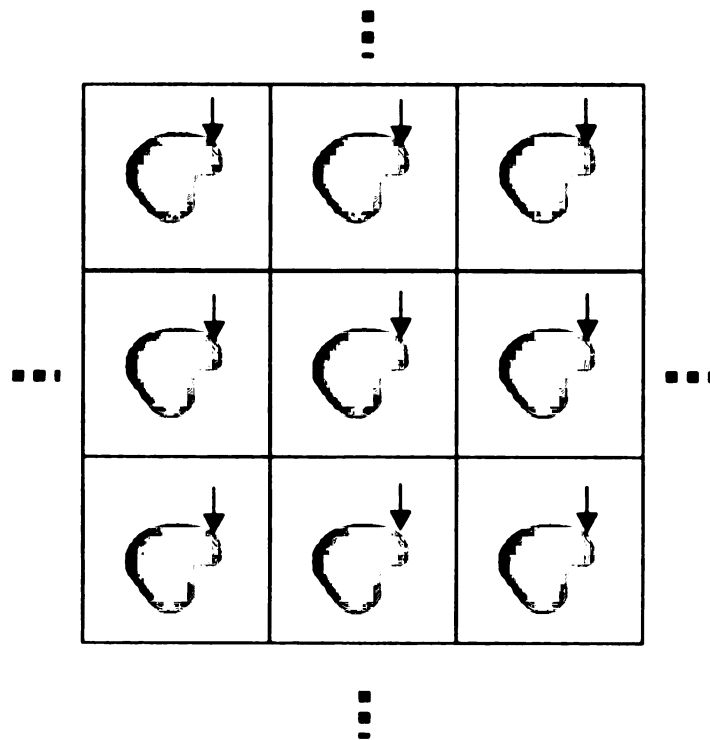


Figure 2.3. Ω -Periodic domain

Convergence proofs and error estimates relevant to this method can be found in the work of Bakhvalov and Knyazev [9].

Our goal is to obtain solutions \mathbf{u} to the Ω -periodic problem that are sufficiently close to \mathbf{v} in Ω_2 . To accomplish this we would like the material in the fictitious domain to have little effect, if any, on the solution in Ω_2 . In the elasticity problem this is guaranteed by requiring that the fictitious domain be composed of a very weak material. The material tensor in the heterogeneous domain Ω is given as

$$\mathbf{D}_\Omega(x, y) = \begin{cases} \mathbf{D}_{\text{weak}} & x, y \in \Omega_1 \\ \mathbf{D}_{\Omega_2}(x, y) & x, y \in \Omega_2 \end{cases} \quad (2.14)$$

Similarly, the mass-density distribution is given as

$$\rho_\Omega(x, y) = \begin{cases} \rho_{\text{weak}} & x, y \in \Omega_1 \\ \rho_{\Omega_2}(x, y) & x, y \in \Omega_2 \end{cases} \quad (2.15)$$

\mathbf{D}_{weak} and ρ_{weak} are properties of the material in the fictitious domain.

Typically, we assume

$$0 < \mathbf{D}_{\text{weak}} \ll \mathbf{D}_{\Omega_2}, \text{ and } 0 < \rho_{\text{weak}} \ll \rho_{\Omega_2} \quad (2.16)$$

and that \mathbf{D}_{weak} is isotropic.

2.4 Summary

We have now successfully formulated an equivalent problem in a regular domain in place of the original problem. This has been done at the price of having significantly increased the size of the problem this fact is illustrated

in Figure 2.4. Thus we need some special solution techniques so that the convergence of the solution process is independent of the size of the problem.

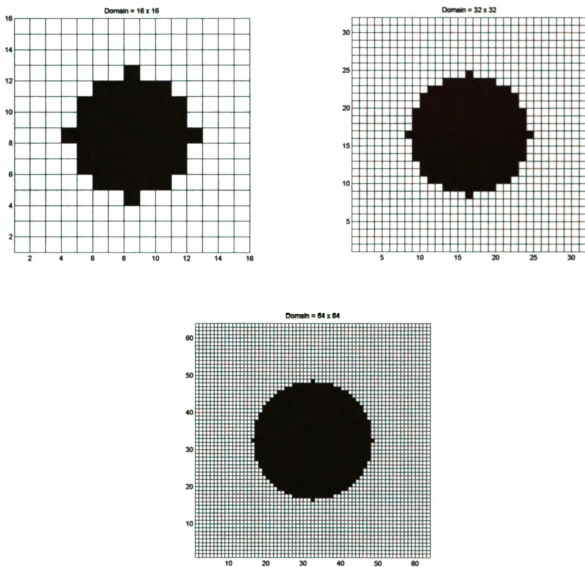


Figure 2.4 A circular domain at various resolutions

Chapter 3

Applying Fictitious Domain Methods To Solve Frequency Response Problems in Two- Dimensions.

3.1 Introduction

This chapter discusses the solution of two dimensional frequency response problems using fictitious domain techniques. In frequency response analysis, the goal is to determine the behavior of a structure subjected to a periodic forcing function with specified boundary conditions or constraints.

The approach discussed in the following sections uses a fictitious domain to recast a given frequency response problem in elasticity with an arbitrary

domain into a periodic problem with a simple, regular domain. Some examples are shown which illustrate the approach.

3.2 Field Equations in Elastodynamics

In this case the equilibrium equations are given as

$$\sigma_{ji,j} + f_i = \rho \ddot{u}_i \quad (3.1)$$

The strain-displacement relations and the stress-strain relationships are the same as those given in equations 2.2 and 2.3. Here, ρ is the mass-density.

Combining equation 3.1 with equations 2.2 and 2.3 we get

$$D_{ijkl} u_{i,jk} + f_i = \rho \ddot{u}_i \quad (3.2)$$

Multiplying this equation with a weight function (\mathbf{w}) and integrating over the volume we get the weak form, which is

$$\int_V \rho \mathbf{w} \ddot{\mathbf{u}} dV + \int_V \mathbf{D} \boldsymbol{\varepsilon}(\mathbf{u}) \boldsymbol{\varepsilon}(\mathbf{w}) dV = \int_V \mathbf{f}^T \mathbf{w} dV \quad \text{for all } \mathbf{w}_i \in H^1(V) \quad (3.3)$$

We account for damping forces by treating them as a special type of non-conservative body force in the above equation [10]. We assume that the damping force at any point is proportional to the velocity and opposite in direction to the velocity, or

$$f_{d,i} = -C \dot{u}_i \quad (3.4)$$

where C is a constant. Now, substituting this in equation 3.3, we get

$$\int_V \rho \mathbf{w} \ddot{\mathbf{u}} dV + \int_V \mathbf{C} \mathbf{w} \dot{\mathbf{u}} dV + \int_V \mathbf{D} \boldsymbol{\varepsilon}(\mathbf{u}) \boldsymbol{\varepsilon}(\mathbf{w}) dV = \int_V \mathbf{f}^T \mathbf{w} dV \quad \text{for all } \mathbf{w}_i \in H^1(V) \quad (3.5)$$

Since the above equation holds for all $w_i \in H^1(V)$, the coefficients of w_i must be equal to zero, thus, in matrix form,

$$\mathbf{m} \ddot{\mathbf{u}} + \mathbf{c} \dot{\mathbf{u}} + \mathbf{k} \mathbf{u} = \mathbf{f} \quad (3.6)$$

Where \mathbf{k} , \mathbf{m} and \mathbf{c} are the stiffness, mass and damping matrices respectively.

We are concerned only with the steady state solutions to the above equations.

We assume solutions of the form

$$u_j = v_j e^{i\omega t} \quad (3.7)$$

Using the above approximation the discretized equations (3.6) can be written as

$$[\mathbf{k} - \omega^2 \mathbf{m} + i \omega \mathbf{c}] \mathbf{v} = \mathbf{f} \quad (3.8)$$

3.3 Problem Statement

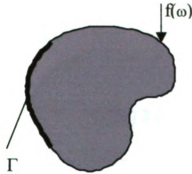


Figure 3.1. Frequency response problem on an arbitrary domain

Figure 3.1 illustrates a typical frequency response problem in elasticity. In the figure Γ is the section of the boundary where the displacement constraints are applied, $f(\omega)$ is the periodic forcing function with ω being the forcing frequency.

The discretized form of the above problem can be mathematically expressed as,

$$\begin{aligned} [\mathbf{k} - \omega^2 \mathbf{m} + i \omega \mathbf{c}] \mathbf{u} &= \mathbf{f} \\ \text{such that } u_i &= 0 \text{ on } \Gamma \end{aligned} \quad (3.9)$$

Here \mathbf{k} is the stiffness matrix, \mathbf{m} is the mass matrix, \mathbf{c} is the damping matrix, \mathbf{f} is the force vector, ω is the forcing frequency and \mathbf{u} is the complex response vector, which contains the magnitude and phase of the displacement.

To solve problem (3.9) using the fictitious domain approach, this arbitrary domain is embedded inside a regular (square) fictitious domain as shown in Figure 3.2.

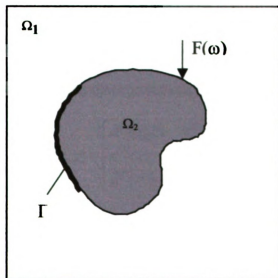


Figure 3.2. Frequency response problem on Ω

Here $\Omega_2 \in \mathbb{R}^2$ is the original arbitrary domain that is embedded in a square fictitious domain $\Omega_1 \in \mathbb{R}^2$ to get a new domain $\Omega = \Omega_1 \cup \Omega_2$, with $\Omega_1 \cap \Omega_2 = \emptyset$. As before the new domain acts as the domain for a new Ω -periodic problem stated as,

$$\mathbf{A}\mathbf{z} = \mathbf{F} \quad (3.10)$$

such that $z_i = 0$ on Γ and \mathbf{z} is periodic

where, $\mathbf{A} = [\mathbf{K} - \omega^2 \mathbf{M} + i\omega \mathbf{C}]$, \mathbf{K} , \mathbf{M} and \mathbf{C} are the stiffness, mass and damping matrices of the new heterogeneous domain Ω , respectively, and \mathbf{z} is the new complex response vector. The constraints in the original problem are enforced in the new fictitious domain problem also.

3.4 Problem Discretization

The domain Ω is treated as a square of dimensions $N \times N$ where $N=2^j$ for a fixed integer j that determines the level of refinement in the approximation. We then designate each unit square $X(k, l) = [k, k+1) \times [l, l+1)$ in Ω as a pixel. This effectively yields a level j , $N \times N$ raster description of the domain.

The material tensor in two-dimensional elasticity has the form

$$\mathbf{D}(x, y) = \begin{bmatrix} d^{11}(x, y) & d^{12}(x, y) & d^{13}(x, y) \\ d^{21}(x, y) & d^{22}(x, y) & d^{23}(x, y) \\ d^{31}(x, y) & d^{32}(x, y) & d^{33}(x, y) \end{bmatrix} \quad (3.11)$$

We simplify the material model by assuming that the material tensor at any location is represented by a scaled version of the fixed isotropic material tensor \mathbf{D}^0 , where \mathbf{D}^0 has the form

$$\mathbf{D}^0 = \frac{E}{(1-\nu^2)} \begin{bmatrix} 1 & \nu & 0 \\ \nu & 1 & 0 \\ 0 & 0 & \frac{1-\nu}{2} \end{bmatrix} \quad (3.12)$$

and E and ν are the Young's modulus and Poisson's ratio respectively.

The material distribution in Ω is now expressed as

$$\mathbf{D}(x, y) = \psi(x, y) \mathbf{D}^0 \quad (3.13)$$

where

$$\psi(x, y) = \begin{cases} \psi_{\text{weak}} & x, y \in \Omega_1 \\ \psi(x, y) & x, y \in \Omega_2 \end{cases} \text{ and } \psi \in (0, 1] \quad (3.14)$$

As discussed earlier, with reasonable choices of the fictitious material tensor, the body force and the constraints set, the solution of the fictitious domain problem (3.10) approaches the solution of the original problem (3.9) in the domain of interest. In addition to the suggested choice of material properties, for the material in the fictitious domain to have little or no effect on the solution in Ω_2 (see equations 2.13-2.15), we also make the ratio of the stiffness tensors to the mass-densities in the fictitious domain much larger compared to those in the actual problem domain. This is done so that the eigenvalues associated with the modes of deformation in the fictitious domain are very large when compared to those in the domain of interest, that is,

$$\frac{1}{\rho_{\text{weak}}} \mathbf{D}_{\text{weak}} \gg \frac{1}{\rho_{\Omega_1}} \mathbf{D}_{\Omega_1} \quad (3.15)$$

A (diagonal) lumped mass matrix is assumed. The damping is assumed to be proportional or Raleigh damping, that is

$$\mathbf{C} = \alpha \mathbf{M} + \beta \mathbf{K} \quad (3.16)$$

where α and β are constants.

3.5 Solution Strategy

In the large-scale problems of interest the discretized system of equations is usually very large and may not be solved by direct methods. We consider a conjugate gradient type method for the solution of the sparse linear system in equation (3.10) with complex symmetric coefficient matrices.

The boundary conditions are applied as in the standard finite element approach, that is, by zeroing out the rows and columns corresponding to the constrained degree of freedom. Mathematically this can be expressed as,

$$\hat{\mathbf{A}} \mathbf{z} = \mathbf{F} \quad (3.17)$$

where, $\hat{\mathbf{A}} = [\mathbf{L} + (\mathbf{I} - \mathbf{L})\mathbf{A}(\mathbf{I} - \mathbf{L})]$, \mathbf{I} is the identity matrix and \mathbf{L} is such that,

$$\begin{aligned} L_{ii} &= 1 \text{ for d.o.f } i \text{ in } \Gamma \text{ (fixed)} \\ L_{ij} &= 0 \text{ otherwise} \end{aligned} \quad (3.18)$$

It is often very enticing to avoid solving complex linear systems by converting them into real systems instead. There are some theoretical and numerical results presented by Freund [11] which show that this is a ‘fatal’ approach, at

least for Krylov subspace methods. In most cases the resulting real systems are harder to solve by the conjugate gradient-type algorithms than the original complex ones. Also the convergence behavior in this case is very erratic.

In this work, one of the simplified quasi-minimal residue (QMR) algorithms for linear systems with J -symmetric or J -Hermitian coefficient matrices has been implemented. This algorithm is one of the simplest possible implementations of the QMR method without look-ahead [12]. This is the quasi-minimal residue from bi-conjugate gradient (QMR-from-BCG) algorithm proposed by Freund and Szeto [13]. By adding updates for the QMR iterates and the QMR search directions and some minor scalar operations to these BCG recursions, they have obtained an algorithm that is only marginally more expensive than BCG and requires one additional matrix-vector product per iteration.

3.6 Preconditioning

The conjugate gradient-type algorithms require an effective preconditioner for rapid convergence. The preconditioner (\mathbf{P}) is a matrix that in some sense approximates the original matrix ($\hat{\mathbf{A}}$) and is easy to invert. This is because the preconditioned conjugate gradient-type algorithms require the inversion of the preconditioner at each step.

Then, for example, the following preconditioned system

$$\mathbf{P}^{-1} \hat{\mathbf{A}} \mathbf{z} = \mathbf{P}^{-1} \mathbf{F} \quad (3.19)$$

could be solved instead of equation (3.17). In general, this system is no longer symmetric. However, we observe that $\mathbf{P}^{-1} \mathbf{A}$ for the \mathbf{P} -inner product $(x, y)_{\mathbf{P}}$ has the property,

$$(x, y)_{\mathbf{P}} \equiv (\mathbf{P}x, y) = (x, \mathbf{P}y) \quad (3.20)$$

since

$$(\mathbf{P}^{-1} \mathbf{A} \mathbf{x}, y)_{\mathbf{P}} = (\mathbf{A} \mathbf{x}, y) = (\mathbf{x}, \mathbf{A} y) = (\mathbf{x}, \mathbf{P}(\mathbf{P}^{-1} \mathbf{A}) y) = (\mathbf{x}, \mathbf{P}^{-1} \mathbf{P} y)_{\mathbf{P}} \quad (3.21)$$

Thus, a simple way of preserving symmetry is to replace the usual Euclidean inner product in the algorithm by the \mathbf{P} -inner product [14].

3.7 Derivation of the Preconditioner

Consider the case where the material distribution in Ω is homogeneous. In this situation, the coefficient matrix $(\mathbf{K}_H - \omega^2 \mathbf{M}_H + i\omega \mathbf{C}_H)$, denoted \mathbf{A}_H , possess some special properties. Each of its sub-matrices in its partitioned structure is an $N^2 \times N^2$ block-circulant matrix

$$\mathbf{A}_H = \begin{bmatrix} \mathbf{A}_{H_{xx}} & \mathbf{A}_{H_{xy}} \\ \mathbf{A}_{H_{yx}} & \mathbf{A}_{H_{yy}} \end{bmatrix} \quad (3.22)$$

A circulant matrix is a square matrix that can be generated from a single row of data. The $(i+1)^{th}$ row of a circulant matrix is generated by performing a circulant shift of the i^{th} row once to the right. An $N^2 \times N^2$ block-circulant

matrix is made up of N^2 blocks of $N \times N$ circulant matrices arranged in a circulant fashion, i.e., the $(i+1)^{th}$ block row is generated by shifting the i^{th} block row once to the right and wrapping around the right end. This is illustrated in Figure 3.3.

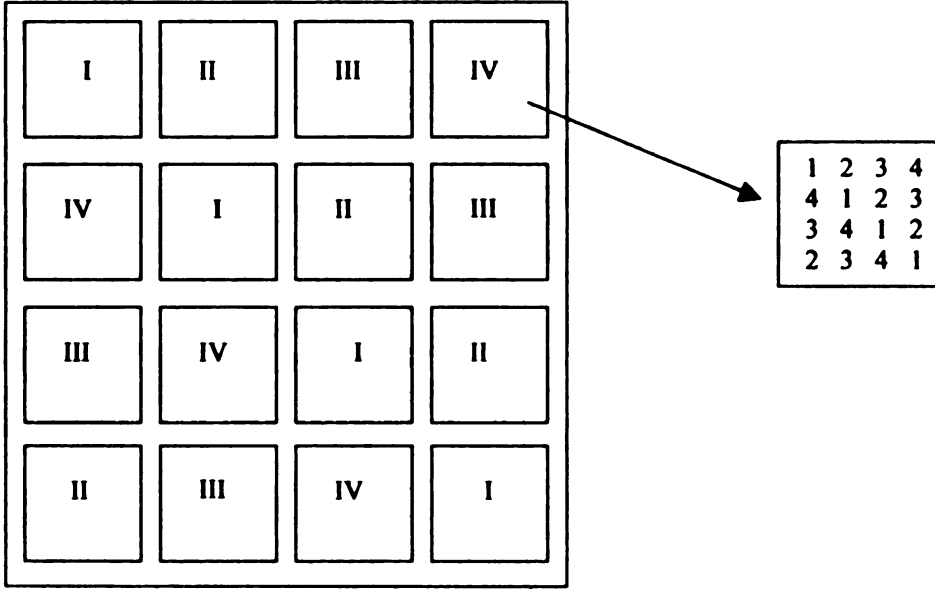


Figure 3.3. Structure of block-circulant matrices

Block-circulant matrices can be stored very efficiently (only one row is needed) and inverted very efficiently using Fourier Transforms [15]. This is due to the fact that block-circulant matrices are diagonal in the Fourier basis. Recalling that each sub-matrix of A_H is block circulant, A_H is tri-diagonal when represented in the Fourier space.

For our particular case a good candidate for the preconditioning matrix (P) would be

$$P = A_H + \kappa L \quad (3.23)$$

where, \mathbf{L} is as described in equation (3.18) and κ is a large penalty parameter. Here, the boundary conditions are applied in the form of a penalty; this is so as to make the inversion of the preconditioner possible as otherwise the matrix would be singular.

3.8 Inversion of the Preconditioner

The inversion of the preconditioning matrix (\mathbf{P}) can be performed very efficiently using a two-step procedure that exploits the fact that \mathbf{A}_H is a symmetric, block-circulant matrix.

First \mathbf{P}^{-1} is expressed as

$$\mathbf{P}^{-1} = [\{(\mathbf{A}_H + \mathbf{p}\mathbf{p}^T) + \kappa\mathbf{B}^T\mathbf{B}\} - \mathbf{p}\mathbf{p}^T]^{-1} \quad (3.24)$$

where

$$\begin{aligned} \mathbf{B}^T\mathbf{B} &= \mathbf{L} \\ \mathbf{P} &= \begin{pmatrix} 1 & \dots & 1 & 0 & \dots & 0 \\ 0 & \dots & 0 & 1 & \dots & 1 \end{pmatrix}^T \end{aligned} \quad (3.25)$$

Here \mathbf{p} is the matrix of rigid body modes of the structure. The matrix $\mathbf{p}\mathbf{p}^T$ is added to \mathbf{A}_H to remove the rigid body mode from the Ω -periodic solution. Matrix $(\mathbf{A}_H + \mathbf{p}\mathbf{p}^T)$ is also symmetric and block-circulant and thus it can be inverted very efficiently using Fourier Transforms. The subtraction of $\mathbf{p}\mathbf{p}^T$ and the addition of $\mathbf{B}^T\mathbf{B}$ are accomplished using the Sherman-Morrison-Woodbury formulae for the matrix inversion of rank-r updates [16]

Given the inverse of a square matrix \mathbf{A} , the Sherman-Morrison formula gives us a way of computing the inverse for changes in \mathbf{A} of the form

$$\mathbf{A} \rightarrow (\mathbf{A} + \mathbf{u} \otimes \mathbf{v}) \quad (3.26)$$

for some vector \mathbf{u} and \mathbf{v} .

$$(\mathbf{A} + \mathbf{u} \otimes \mathbf{v})^{-1} = \mathbf{A}^{-1} - \frac{(\mathbf{A}^{-1}\mathbf{u}) \otimes (\mathbf{v}\mathbf{A}^{-1})}{1 + \lambda} \quad (3.27)$$

where

$$\lambda \equiv \mathbf{v}\mathbf{A}^{-1}\mathbf{u} \quad (3.28)$$

In our case, we want to add more than a single correction term, then the Sherman-Morrison formula cannot be directly applied for the simple reason that the storage of the whole inverse matrix \mathbf{A}^{-1} is not feasible. Instead, we use the Woodbury formula, which is the block matrix form of the Sherman-Morrison formula.

$$(\mathbf{A} + \mathbf{U}\mathbf{V}^T)^{-1} = \mathbf{A}^{-1} - [\mathbf{A}^{-1}\mathbf{U}(\mathbf{I} + \mathbf{V}^T\mathbf{A}^{-1}\mathbf{U})^{-1}\mathbf{V}^T\mathbf{A}^{-1}] \quad (3.29)$$

Here \mathbf{A} is an $n \times n$ matrix, while \mathbf{U} and \mathbf{V} are $n \times p$ matrices with $p < n$ and usually $p \ll n$. The inner part of the correction term whose inverse is needed is only $p \times p$ rather than $n \times n$.

The preconditioner (\mathbf{P}) discussed above has been used in various numerical experiments with success. Examples that illustrate the strategy are presented next.

3.9 Examples

The following section discusses some examples that illustrate our approach and the efficiency of the solver.

3.9.1 Example 1

First, we consider a simple example of a cantilever beam with a tip load. The problem description is as follows.

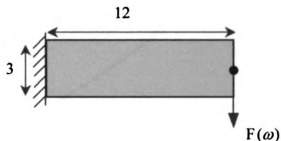


Figure 3.4 Cantilever beam with a tip load

The material properties are as follows, Modulus of Elasticity, $E = 100000$, Poisson's Ratio, $\nu = 0.3$, Mass Density, $\rho = 1$. This is then embedded in a fictitious domain with $E_{fictitious} = 0.1$, $\rho_{fictitious} = 10^{-8}$, $\nu = 0.3$ and solved for the displacements. Figure 3.5 shows the centerline deflection of the cantilever beam obtained from our solution using the fictitious domain technique as well as the exact solution.

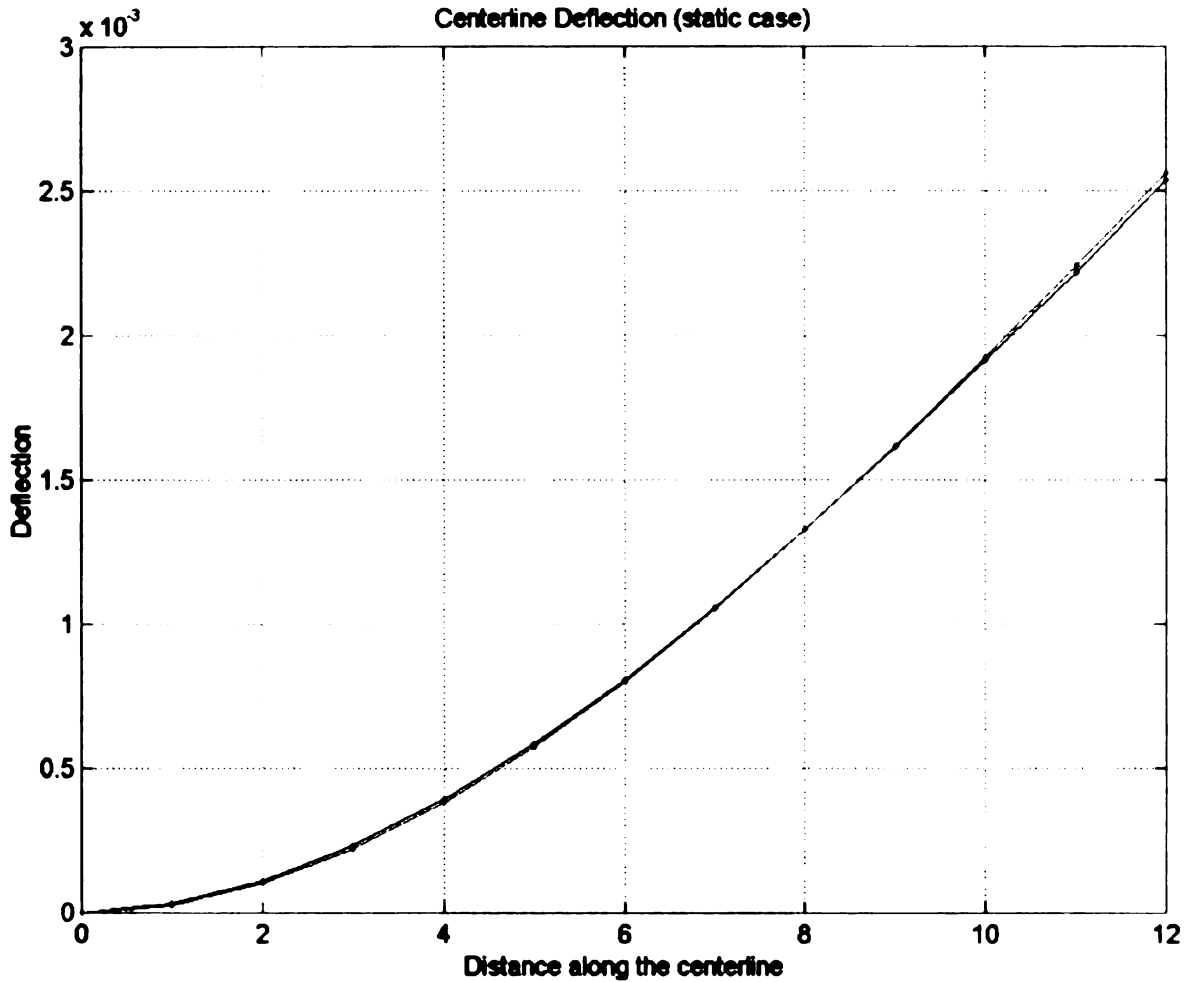


Figure 3.5 Comparison of fictitious domain solution with the exact result

As seen from the above figure, the fictitious domain solution matches very closely with the exact solution for the static case.

Next, we consider the performance of our solver for different preconditioning matrices. We have shown the performance of the solver for three preconditioning matrices namely, the identity matrix, $\mathbf{P}=\mathbf{I}$, i.e., the no-

preconditioning case, a diagonal matrix, $\mathbf{P} = \text{diag}(\mathbf{A})$ and finally the proposed homogeneous coefficient matrix, $\mathbf{P} = \mathbf{A}_H + \kappa \mathbf{L}$.

Figure 3.6 shows the iteration histories these three preconditioning matrices.

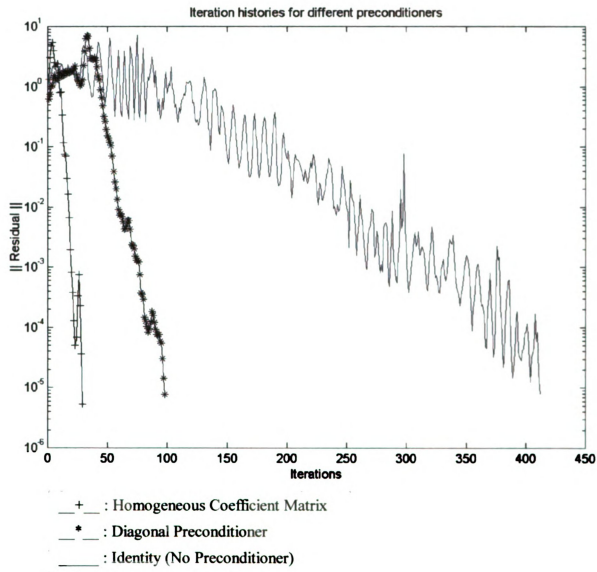
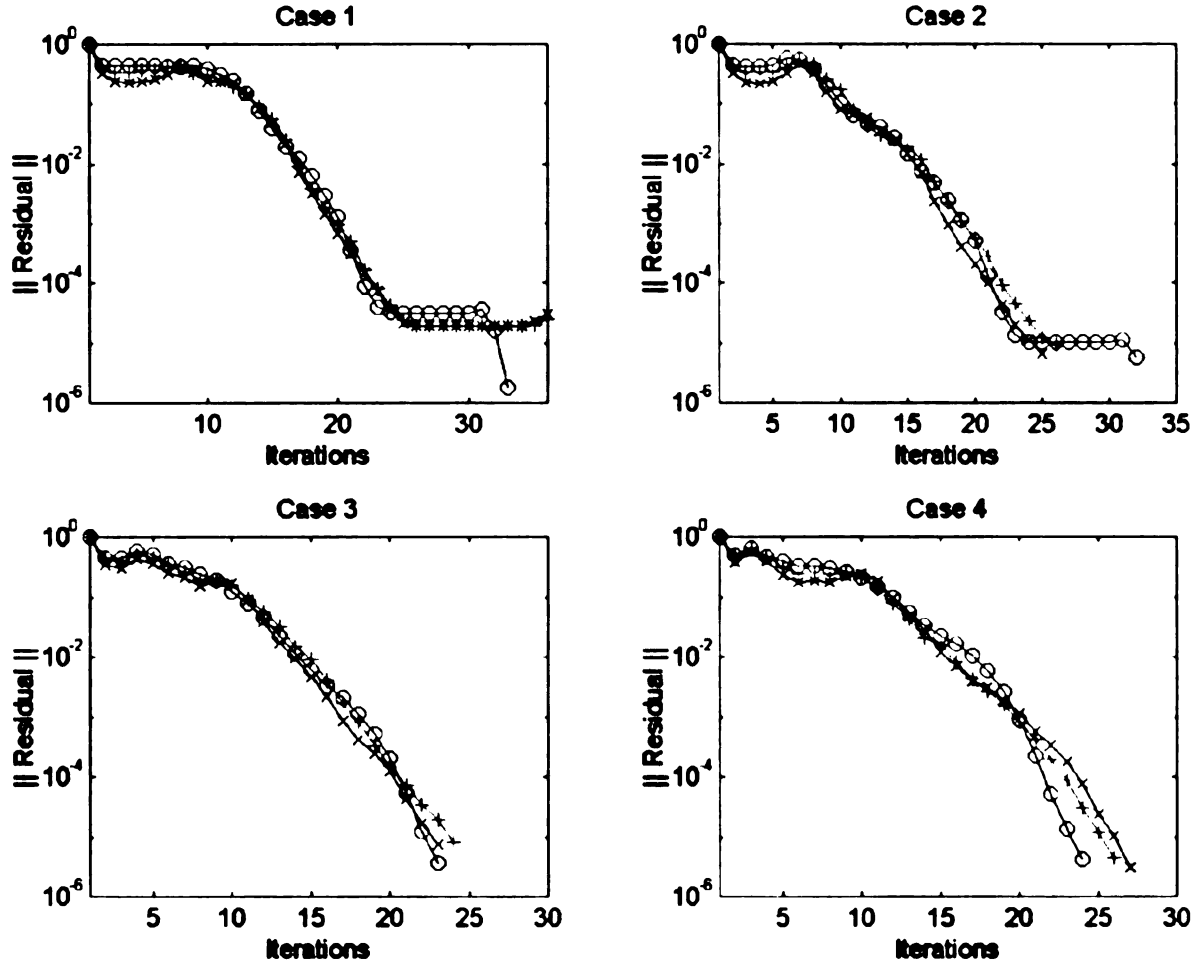


Figure 3.6 Performance of the solver for various preconditioners

It is evident that the proposed homogeneous coefficient matrix is a much better preconditioner than the other two cases. Now we have to show that this method works equally well for different resolutions of the domain, i.e. different sizes of the coefficient matrix. This is shown in the Figure 3.7, where the iteration histories for different resolutions and different forcing frequencies are plotted.



___o___ : Domain is 16×16 (512 degrees of freedom)
 ___+___ : Domain is 32×32 (2048 degrees of freedom)
 ___x___ : Domain is 64×64 (8192 degrees of freedom)

Case 1 : $\omega = 5$
 Case 2 : $\omega = 10$
 Case 3 : $\omega = 20$
 Case 4 : $\omega = 30$

Figure 3.7 Performance of the solver for different frequencies and resolutions.

The above figure shows the iterations converge at around the same number of iterations, unlike standard finite element methods, where the slope of the iteration curve would decrease proportional to the increase in the resolution. It is also noted that for higher frequencies the iterations converge rapidly, as is expected since, now, the mass matrix becomes more dominant and in our case the mass matrix is diagonal.

Figure 3.8 shows the frequency response plot taken at the tip of the cantilever beam. The figure shows the frequency response obtained by using our fictitious domain method as well as that obtained from a standard finite element method. The solution using the fictitious domain technique matches exactly with the solution from ANSYS for level6 (64×64), thus confirming the accuracy of the solver at high levels of resolution.

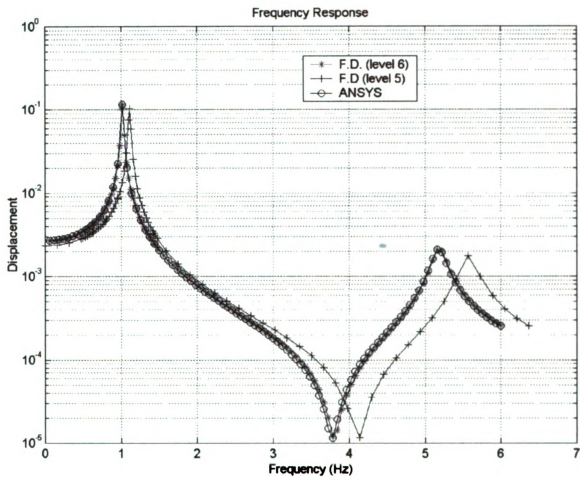


Figure 3.8 Frequency response plots

3.9.2 Example 2

The next example we consider is a rectangular plate with a hole in the center and with a horizontal force at the edges. The problem description is shown as follows.

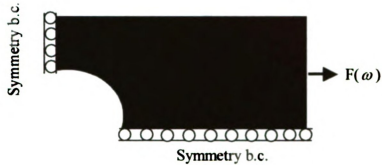


Figure 3.9 One quarter of a plate with a center hole

The material properties are as follows,

Modulus of Elasticity, $E = 100000$

Poisson's Ratio, $\nu = 0.3$

Mass Density, $\rho = 1$

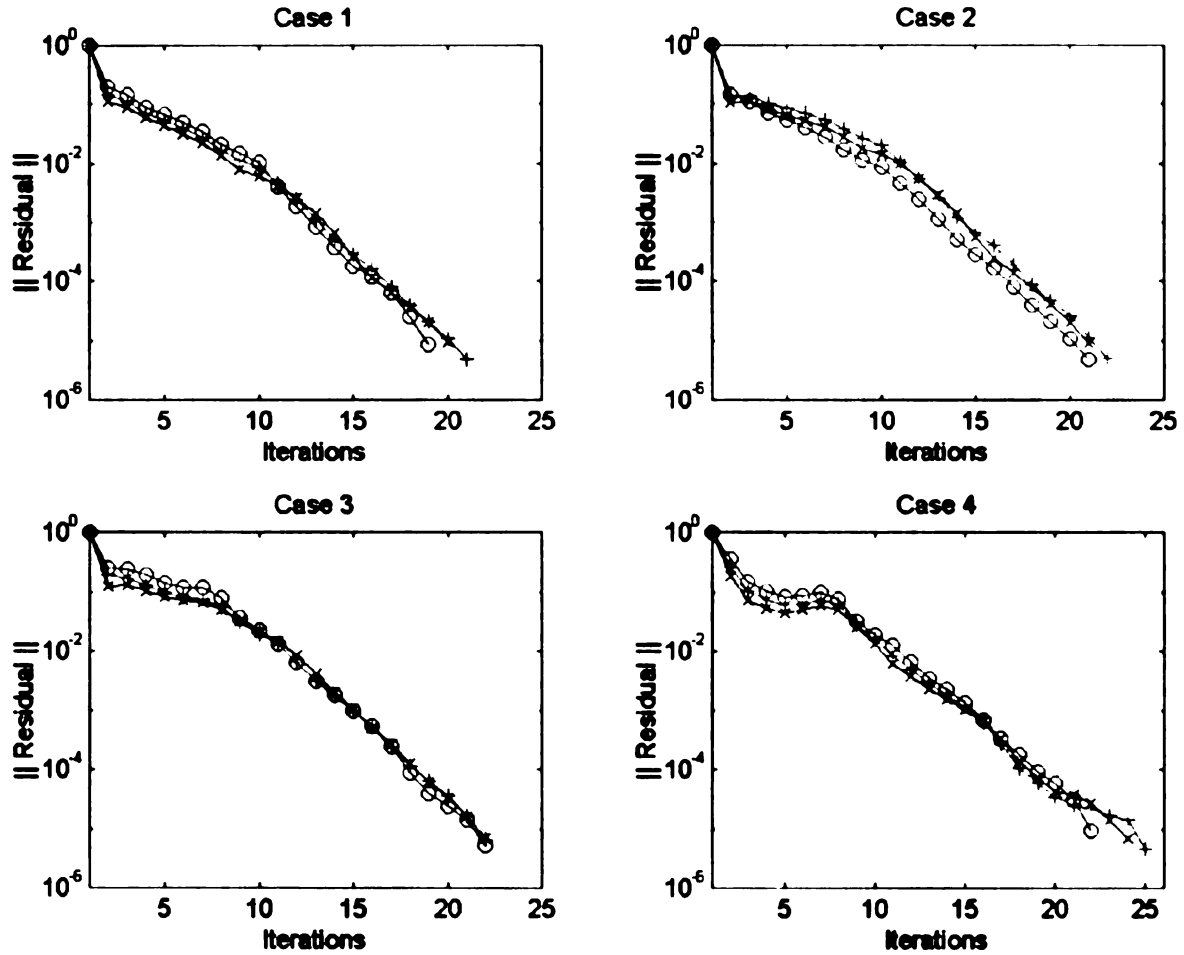
This is embedded in a fictitious domain with the following material properties,

Modulus of Elasticity, $E_{fictitious} = 0.1$

Poisson's Ratio, $\nu = 0.3$

Mass Density, $\rho_{fictitious} = 10^{-8}$

Figure 3.10 shows the iteration history for this problem for three different levels of resolution and for four forcing frequencies.



___o___ : Domain is 32×32 (2048 degrees of freedom)
 ___+___ : Domain is 64×64 (8192 degrees of freedom)
 ___x___ : Domain is 128×128 (32768 degrees of freedom)

Case 1 : $\omega = 5$
 Case 2 : $\omega = 10$
 Case 3 : $\omega = 20$
 Case 4 : $\omega = 30$

Figure 3.10 Performance of the solver for different frequencies and resolutions.

The above figure shows that the number of iterations taken to converge is fairly low as compared to the number of degrees of freedom and also it does not vary much with the increase in the number of degrees of freedom.

Figure 3.11 shows the frequency response plot taken at a point on the edge of the plate. As observed earlier, the fictitious domain solution matches the finite element solution as the level of resolution of the domain increases.

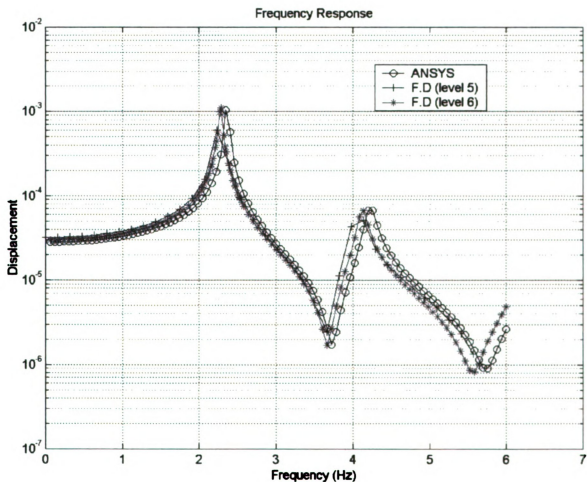


Figure 3.11 Frequency response plot

3.9.3 Example 3

Here we consider a curved beam, fixed at one end and a horizontal load at the other as shown in Figure 3.12.

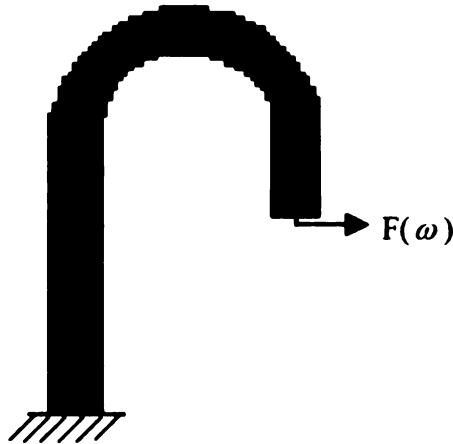


Figure 3.12 A curved beam, fixed at one end and a tip load at the other

The material properties are as follows,

Modulus of Elasticity, $E = 100000$

Poisson's Ratio, $\nu = 0.3$

Mass Density, $\rho = 1$

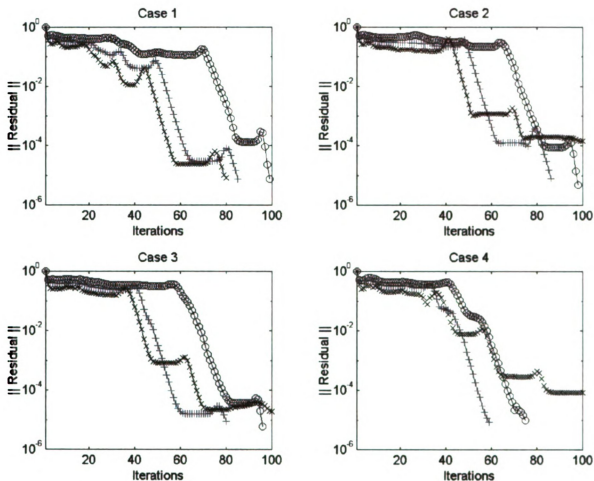
This is embedded in a fictitious domain with the following material properties,

Modulus of Elasticity, $E_{fictitious} = 0.1$

Poisson's Ratio, $\nu = 0.3$

Mass Density, $\rho_{fictitious} = 10^{-8}$

Figure 3.13 shows the convergence behavior for three different resolutions of the domain and for four forcing frequencies.



o : Domain is 32×32 (2048 degrees of freedom)
+ : Domain is 64×64 (8192 degrees of freedom)
x : Domain is 128×128 (32768 degrees of freedom)

Case 1 : $\omega = 0.1$
Case 2 : $\omega = 0.5$
Case 3 : $\omega = 1.0$
Case 4 : $\omega = 2.0$

Figure 3.13 Performance of the solver for different frequencies and resolutions.

Figure 3.14 shows the frequency response taken at the free end of the beam.

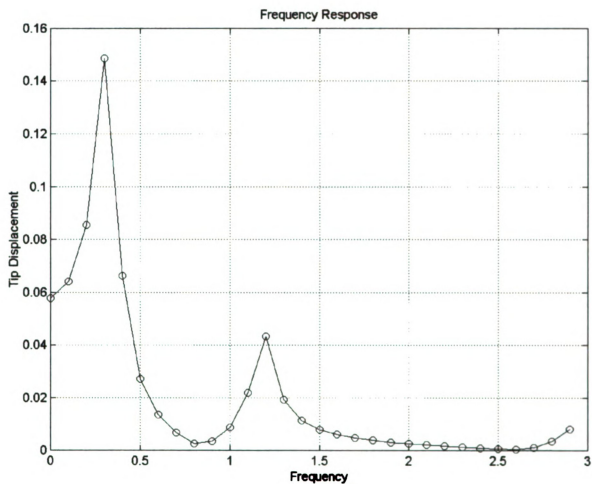


Figure 3.14 Frequency response plot

3.9.4 Example 4

Finally, we consider this “arbitrary” geometry shown in Figure 3.15 to show that our solver does not require any kind of meshing that is adapted to individual geometries. This domain was drawn using a commercial image processing software and that image itself serves as the input to the program, no other form of adapting of the drawing is required.



Figure 3.15 An arbitrary geometry fixed at two ends and a force in the middle

The material properties are as follows,

Modulus of Elasticity, $E = 100000$

Poisson's Ratio, $\nu = 0.3$

Mass Density, $\rho = 1$

This is embedded in a fictitious domain with the following material properties,

Modulus of Elasticity, $E_{fictitious} = 0.1$

Poisson's Ratio, $\nu = 0.3$

Mass Density, $\rho_{fictitious} = 10^{-8}$

Figure 3.16 shows the convergence behavior for different resolutions of the domain and for different forcing frequencies.

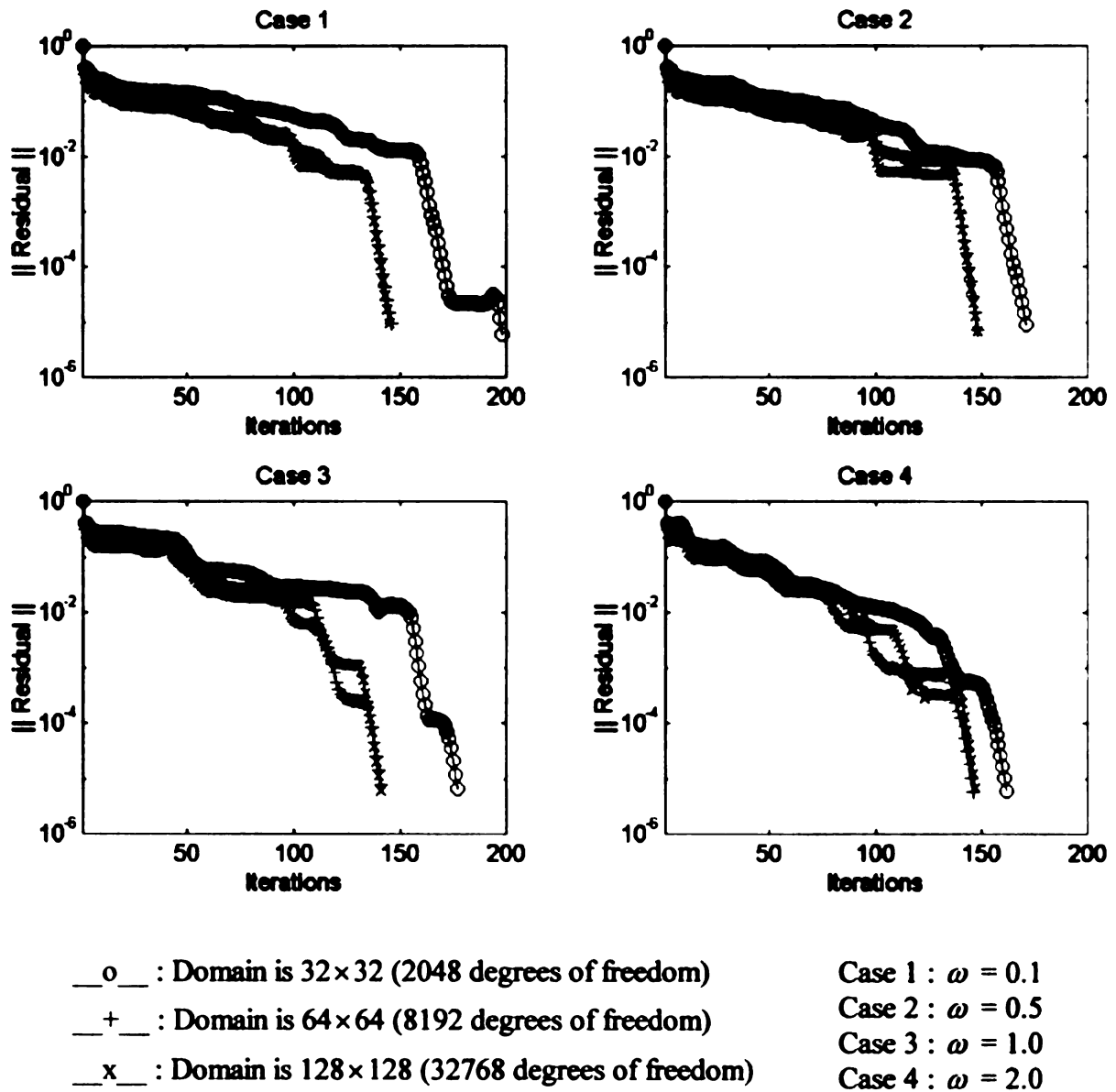


Figure 3.16 Performance of the solver for different frequencies and resolutions.

Figure 3.17 shows the plot of the frequency response at the point where the force is applied.

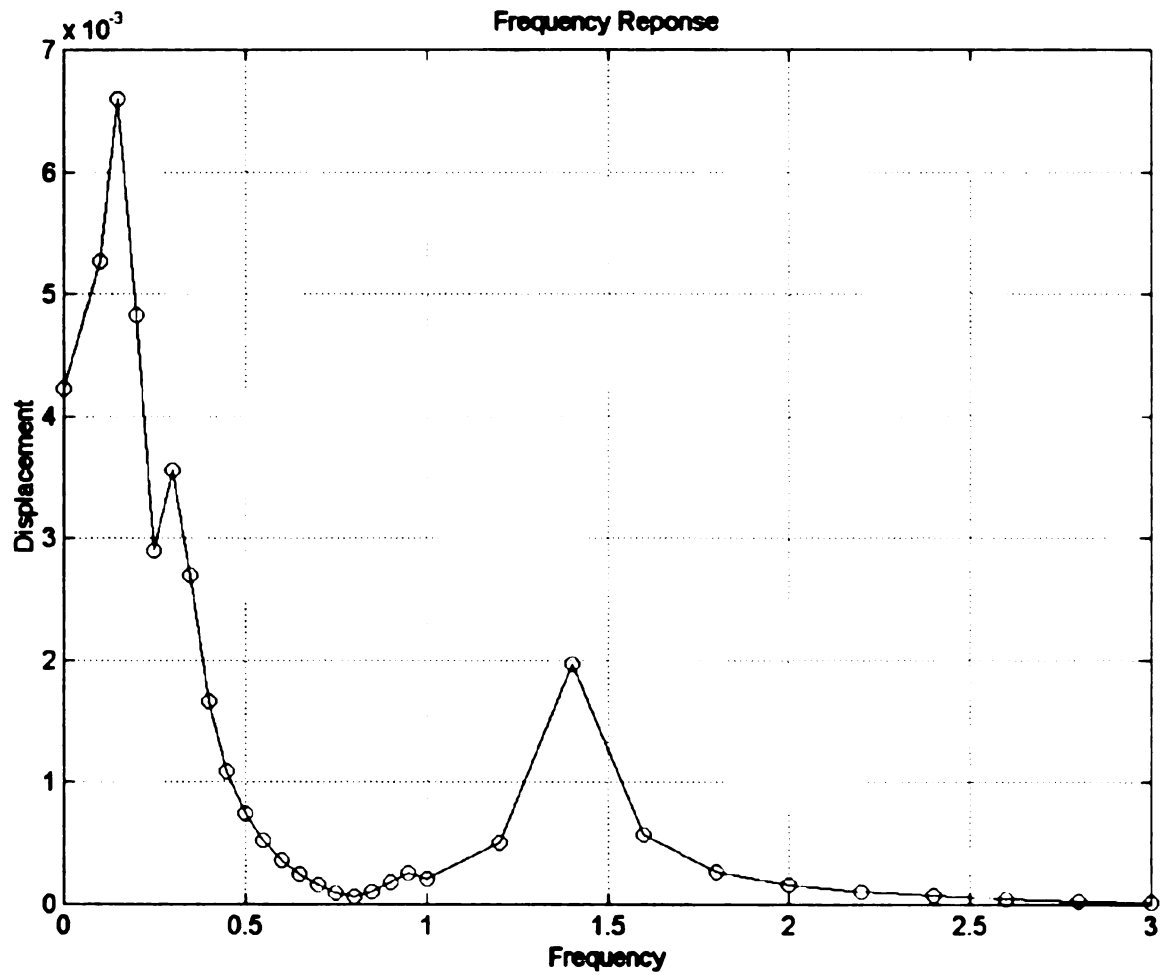


Figure 3.17 Frequency response plot

Chapter 4

Solving frequency response problems in three dimensions.

4.1 Introduction

This chapter discusses the application of the fictitious domain method to solve three-dimensional frequency response problems. An overview of the problem statement and the discretization process in three dimensions is followed by the solution technique associated with the three-dimensional problem. Examples solved using this method are discussed.

4.2 Problem Statement

Consider a three-dimensional frequency response problem in elasticity on an arbitrarily shaped domain $\Omega_2 \in \mathbb{R}^3$ with boundary conditions specified on

$\Gamma \subset \partial\Omega_2$. Like its two-dimensional counterpart, this problem in its discretized form can be expressed mathematically as

$$\begin{aligned} [\mathbf{k} - \omega^2 \mathbf{m} + i\omega \mathbf{c}] \mathbf{u} &= \mathbf{f} \\ \text{such that } u_i &= 0 \text{ on } \Gamma \end{aligned} \tag{4.1}$$

Note that $\mathbf{u} = (u_x, u_y, u_z)$, $\mathbf{f} = (f_x, f_y, f_z)$.

To solve the above problem using the fictitious domain technique, the domain of interest Ω_2 is embedded into a cube Ω_1 to give a new domain Ω and the added region, $\Omega_1 = \Omega \setminus \Omega_2$ is filled with a weak material. As before, an approximate solution for the elasticity problem in the original domain Ω_2 is extracted from an Ω -periodic solution to the problem shown in 4.2.

$$\begin{aligned} \mathbf{A} \mathbf{z} &= \mathbf{F} \\ \text{such that } z_i &= 0 \text{ on } \Gamma \text{ and } \mathbf{z} \text{ is periodic} \end{aligned} \tag{4.2}$$

where, $\mathbf{A} = [\mathbf{K} - \omega^2 \mathbf{M} + i\omega \mathbf{C}]$, \mathbf{K} , \mathbf{M} and \mathbf{C} are the stiffness, mass and damping matrices of the new domain Ω . The constraints on the original problem are enforced here too.

As seen from the discussion in two dimensions, for sufficiently weak fictitious material property and proper representation of the boundary and loading conditions, the solution in the periodic problem Ω is a good approximation of the solution in the original problem Ω_2 . We now discuss the discretization and the solution of the fictitious domain problem in three dimensions.

4.3 Problem Discretization In Three Dimensions

The fictitious domain in three dimensions is discretized using small cubes or voxels, the three-dimensional equivalent of pixels in two dimensions. Voxels are indexed in raster form where $X(k,l,m)$ corresponds to the voxel occupying the unit cube $[k,k+1) \times [l,l+1) \times [m,m+1)$. This results in an $N \times N \times N$ voxel discretization of Ω as shown in figure 4.1. Again we select $N = 2^j$ for a fixed positive integer j .

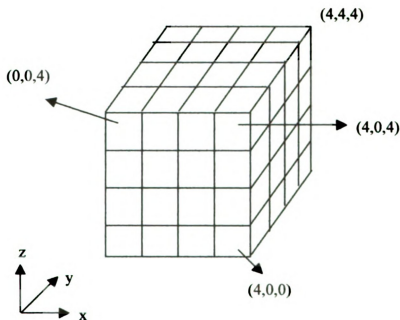


Figure 4.1 Example of voxel discretization

The material tensor in three dimensions has the form,

$$\mathbf{D}(x, y, z) = \begin{bmatrix} E_{1111} & E_{1122} & E_{1133} & E_{1123} & E_{1113} & E_{1112} \\ E_{1122} & E_{2222} & E_{2233} & E_{2223} & E_{2213} & E_{2212} \\ E_{1133} & E_{2233} & E_{3333} & E_{3323} & E_{3313} & E_{3312} \\ E_{1123} & E_{2223} & E_{3323} & E_{2323} & E_{2313} & E_{2312} \\ E_{1113} & E_{2213} & E_{3313} & E_{2313} & E_{1313} & E_{1312} \\ E_{1112} & E_{2212} & E_{2312} & E_{1312} & E_{1312} & E_{1212} \end{bmatrix} \quad (4.3)$$

where E_{ijkl} are functions of the spatial coordinates x, y and z .

Using the simplified model as in the case of two dimensions, the material tensor at any location is represented by a scaled version of the fixed isotropic material tensor \mathbf{D}^0 , where \mathbf{D}^0 is of the form

$$\mathbf{D}^0 = \frac{E}{(1+\nu)(1-2\nu)} \begin{bmatrix} 1-\nu & \nu & \nu & 0 & 0 & 0 \\ \nu & 1-\nu & \nu & 0 & 0 & 0 \\ \nu & \nu & 1-\nu & 0 & 0 & 0 \\ 0 & 0 & 0 & \frac{1-2\nu}{2} & 0 & 0 \\ 0 & 0 & 0 & 0 & \frac{1-2\nu}{2} & 0 \\ 0 & 0 & 0 & 0 & 0 & \frac{1-2\nu}{2} \end{bmatrix} \quad (4.4)$$

E and ν are the Young's modulus and the Poisson's ratio respectively.

The material distribution in Ω is now expressed as

$$\mathbf{D}(x, y, z) = \psi(x, y, z) \mathbf{D}^0 \quad (4.5)$$

and

$$\psi(x, y, z) = \begin{cases} \psi_{\text{weak}} & x, y, z \in \Omega_1 \\ \psi(x, y, z) & x, y, z \in \Omega_2 \end{cases} \quad (4.6)$$

The criteria used for the judicious choice of the material property in the fictitious domain in two dimensions apply here also.

4.4 Solution Strategy

As before, we consider a preconditioned conjugate gradient type method for the solution of the sparse system of equations (4.2) with complex symmetric coefficient matrices. The fictitious domain method adds a number of degrees of freedom to the original problem, but we are not concerned with the response at any of these “fictitious” degrees of freedom. The solution technique used for the two-dimensional case treats these degrees of freedom also on par with degrees of freedom in the problem domain, thus, wasting the computational resources to compute the response at a degree of freedom that is fictitious, i.e., in regions of no physical meaning. We now propose another more memory and computation efficient solution technique for the three-dimensional problems by imposing additional constraints on the fictitious domain problem to zero-out the response at the fictitious degrees of freedom. The fictitious domain problem now becomes,

$$\hat{\mathbf{A}}\mathbf{z} = \mathbf{F} \quad (4.7)$$

Where, $\hat{\mathbf{A}} = [\mathbf{N} + (\mathbf{I} - \mathbf{N})\mathbf{A}(\mathbf{I} - \mathbf{N})]$, \mathbf{I} is the identity matrix and \mathbf{N} is such that,

$$N_{ii} = \begin{cases} 1, & \text{for degree of freedom } i \in \Gamma \\ 1, & \text{for degree of freedom } i \in \Phi \end{cases} \quad (4.8)$$

$$N_{ij} = 0, \text{ otherwise}$$

Here, $\Gamma \subset \partial\Omega_2$ is the set of constrained degrees of freedom in the original problem domain and Φ is the set of fictitious degrees of freedom, the two-dimensional version of this is shown in figure 4.2.

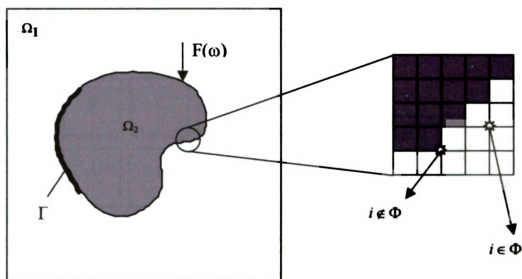


Figure 4.2. Constrained and Fictitious degrees of freedom

4.5 Derivation of the Preconditioner

Here again we examine the coefficient matrix associated with the case where the domain Ω contains an isotropic, homogeneous material, denoted as $\mathbf{A}_H \left(= \left[\mathbf{K}_H - \omega^2 \mathbf{M}_H + i\omega \mathbf{C}_H \right] \right)$ shown in equation (4.9) in its partitioned form.

$$\mathbf{A}_H = \begin{bmatrix} \mathbf{A}_{H_{xx}} & \mathbf{A}_{H_{xy}} & \mathbf{A}_{H_{xz}} \\ \mathbf{A}_{H_{yx}} & \mathbf{A}_{H_{yy}} & \mathbf{A}_{H_{yz}} \\ \mathbf{A}_{H_{zx}} & \mathbf{A}_{H_{zy}} & \mathbf{A}_{H_{zz}} \end{bmatrix} \quad (4.9)$$

Recall that in the two-dimensional case, the sub-matrices of the homogeneous matrix were block circulant. In three dimensions, the partitions of the homogeneous coefficient matrix A_{H_u} are two-block circulant matrices. This means that each matrix A_{H_u} is block circulant and its block matrices themselves are block circulant, this is shown in the figure-4.3.

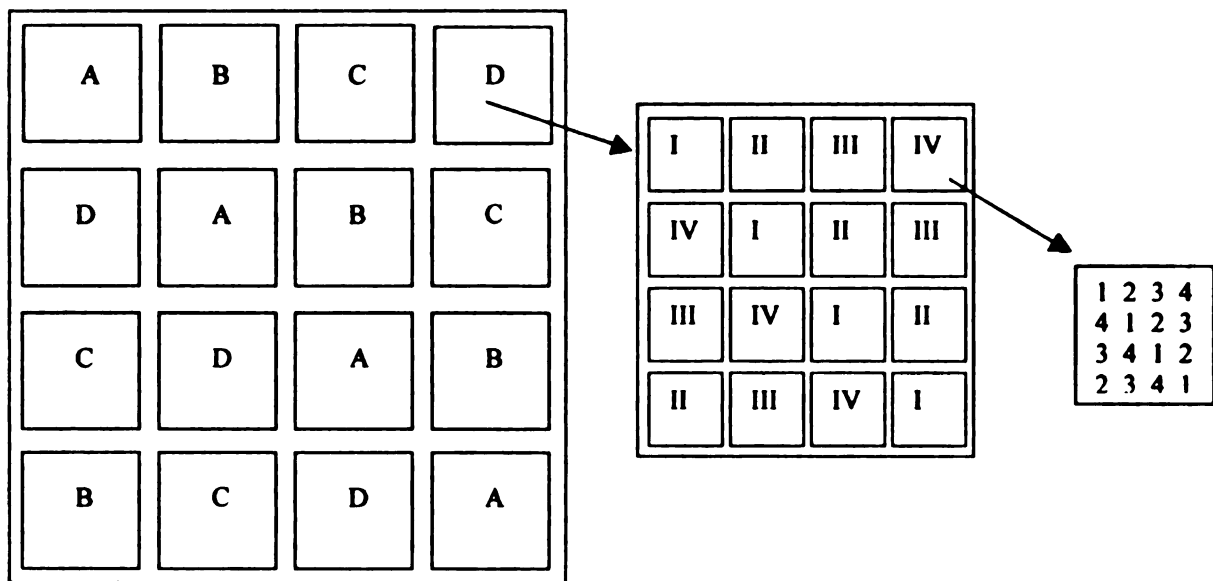


Figure 4.3. Structure of two-block circulant matrices

Fortunately, two-block circulant matrices are also diagonal when represented in the Fourier space and a simple three-dimensional Fourier transform can diagonalize the sub-matrices of A_H . Recall, that a preconditioner is a matrix that closely resembles the original matrix to be inverted (\hat{A}) and one that can be inverted easily. Ideally, a first choice for the preconditioning matrix would be

$$\mathbf{P} = [\mathbf{N} + (\mathbf{I} - \mathbf{N}) \mathbf{A}_H (\mathbf{I} - \mathbf{N})] \quad (4.10)$$

This has the effect of deleting rows and columns of \mathbf{A}_H associated with non-zero entries in \mathbf{N} . \mathbf{N} is as defined in equation (4.8) and \mathbf{I} is the identity matrix. Due to the elimination of rows and columns in \mathbf{A}_H , this matrix is no longer block circulant and cannot be inverted easily using Fourier transforms. Thus essentially the advantage of \mathbf{A}_H being block circulant is lost. Thus this is not a good choice. Our aim now is to find a preconditioning matrix that takes advantage of the block circulant nature of the homogeneous coefficient matrix and whose spectrum is similar to that of the original matrix whose inverse needs to be computed.

We now define

$$\mathbf{A}_\varepsilon = (\mathbf{A}_H + \kappa \mathbf{L}) + \varepsilon \mathbf{Q} \quad (4.11)$$

Where, \mathbf{A}_H is the homogeneous coefficient matrix with the modulus of elasticity being unity and an identity mass matrix, ε is a small number and κ is a large penalty. \mathbf{L} is a diagonal matrix with the diagonal entry being unity at a constrained degree of freedom and zeros elsewhere, \mathbf{Q} is added to remove the three rigid body modes associated with the three-dimensional problems as shown in equations (4.12) and (4.13).

$$\begin{aligned} L_{ii} &= 1 \text{ for } i \text{ in } \Gamma \text{ (i.e. fixed d.o.f)} \\ L_{ij} &= 0 \text{ otherwise} \end{aligned} \quad (4.12)$$

$$\mathbf{Q} = \mathbf{p} \mathbf{p}^T \quad (4.13)$$

Here, \mathbf{p} is the matrix consisting of three columns of the rigid body modes ($\hat{\mathbf{p}}$) normalized in such a way that $\mathbf{p}^T \mathbf{p} = \mathbf{I}_{3 \times 3}$.

$$\hat{\mathbf{p}} = \begin{pmatrix} 1 & \dots & 1 & 0 & \dots & 0 & 0 & \dots & 0 \\ 0 & \dots & 0 & 1 & \dots & 1 & 0 & \dots & 0 \\ 0 & \dots & 0 & 0 & \dots & 0 & 1 & \dots & 0 \end{pmatrix}^T \quad (4.14)$$

From these, we can see that the three non-zero eigenvalues of \mathbf{Q} are equal to one.

Now, we approximate the inverse of the preconditioner to be,

$$\mathbf{P}_\epsilon^{-1} = [\mathbf{N} + (\mathbf{I} - \mathbf{N}) \mathbf{A}_\epsilon^{-1} (\mathbf{I} - \mathbf{N})] \quad (4.15)$$

Note that \mathbf{A}_ϵ is not a block circulant matrix, but is a rank update of a block circulant matrix ($\mathbf{A}_H + \epsilon^* \mathbf{Q}$). As before, the update \mathbf{L} can be expressed as a product,

$$\mathbf{L} = \mathbf{B} \mathbf{B}^T \quad (4.16)$$

To invert \mathbf{A}_ϵ , we use the Sherman-Morrison-Woodbury formulae as we have done in the two-dimensional case.

The preconditioner discussed above has been used in various numerical experiments with success. Examples that illustrate this strategy are presented next.

4.6 Examples

The following section discusses some examples that illustrate our approach and the efficiency of the solver.

4.6.1 Example 1

The first example considered is a bar that is clamped at one end and a tip load at the other as shown in Figure 4.4.

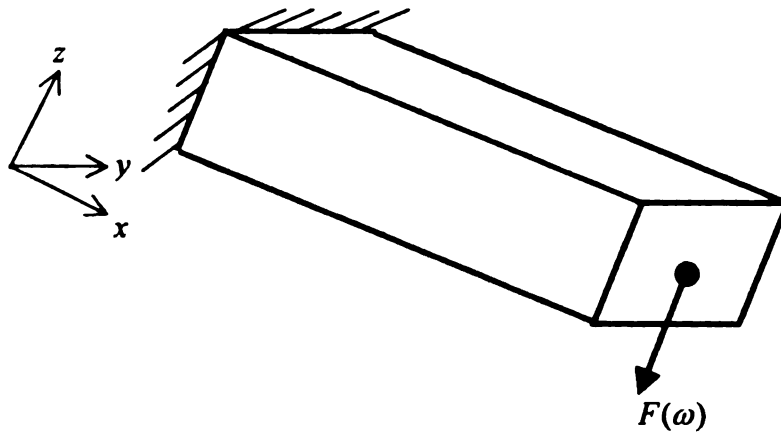


Figure 4.4 a rectangular bar with a tip load

The material properties are as follows,

Modulus of Elasticity, $E = 100000$

Poisson's Ratio, $\nu = 0.3$

Mass Density, $\rho = 1$

$$\frac{E}{\rho} = 10^5$$

Figure 4.5 shows the iteration history for this problem for different levels of resolution and frequency.

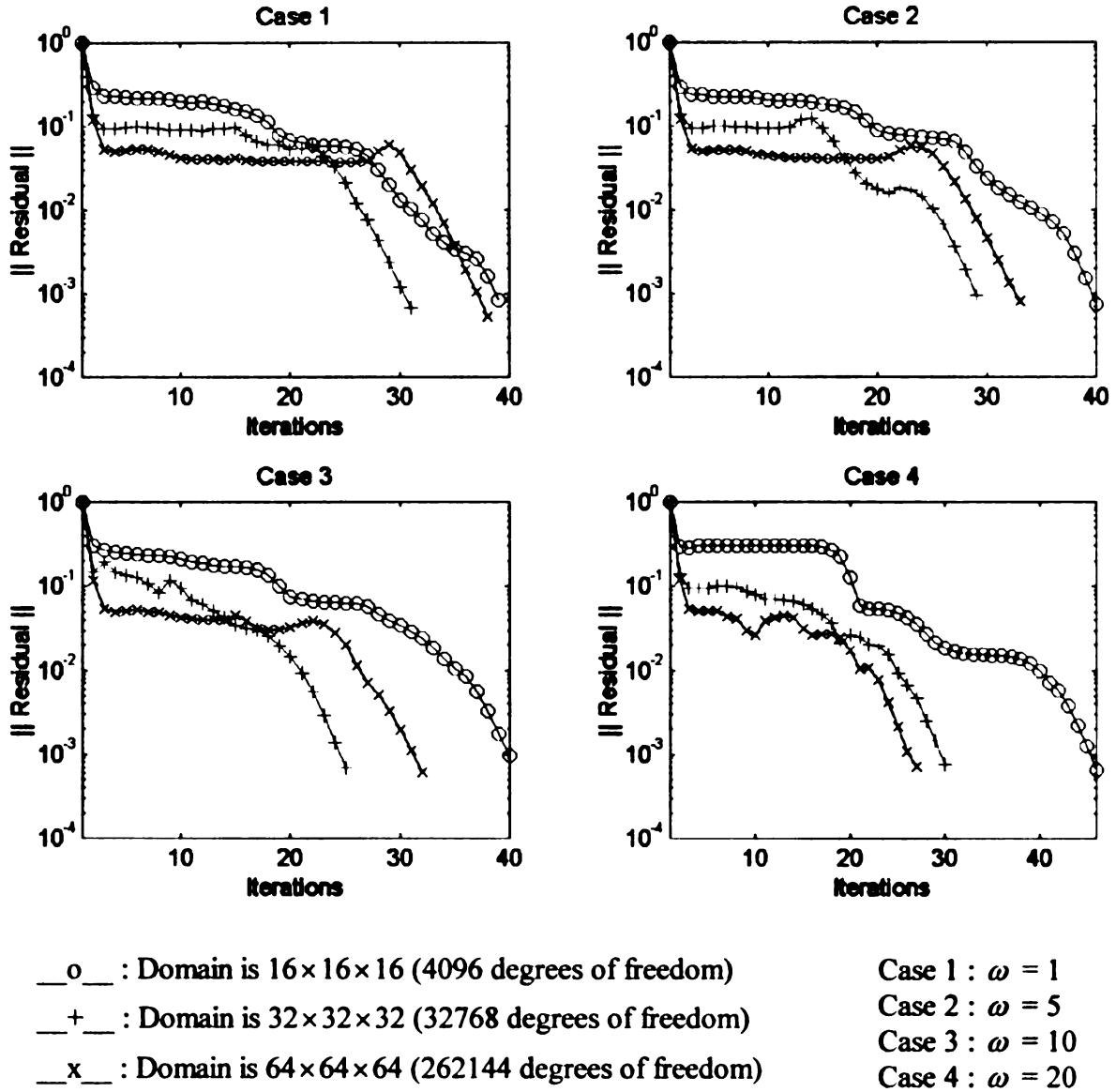


Figure 4.5 Performance of the solver for different frequencies and resolutions.

It can be seen from the above figure that the convergence rate remains in the same order of magnitude for the three levels of resolution of the domain.

Figure 4.6 shows the frequency response plot obtained using the fictitious domain method as well as that obtained using a commercial finite element software (ANSYS).

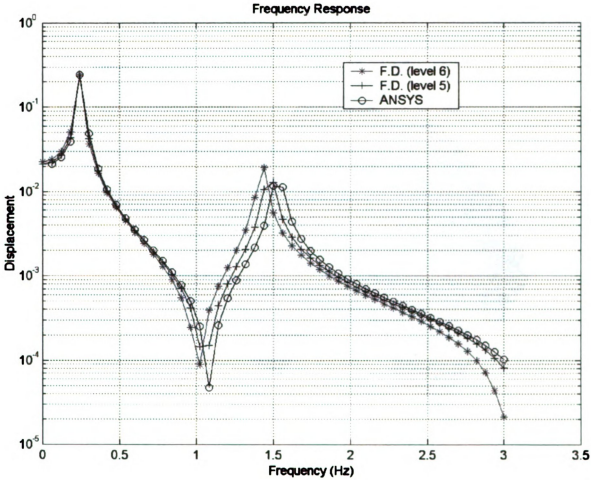


Figure 4.6 Frequency response plots

As in the two-dimensional case the solution obtained from the fictitious domain method matches well with the solution from standard finite element method.

4.6.2 Example 2

The next example considered is a crankshaft, the problem description is as shown in Figure 4.7

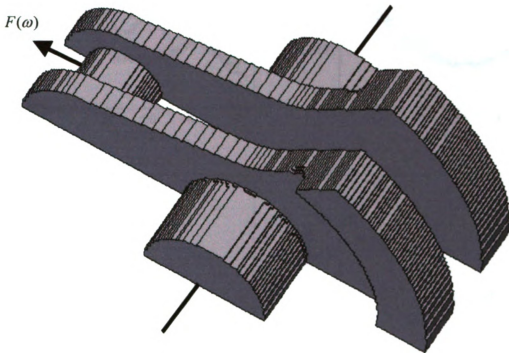


Figure 4.7 One half of a crankshaft, constrained along its length

The material properties are as follows,

Modulus of Elasticity, $E = 100000$

Poisson's Ratio, $\nu = 0.3$

Mass Density, $\rho = 1$

$$\frac{E}{\rho} = 10^5$$

Figure 4.8 shows the iteration history for this problem for different levels of resolution and frequency.

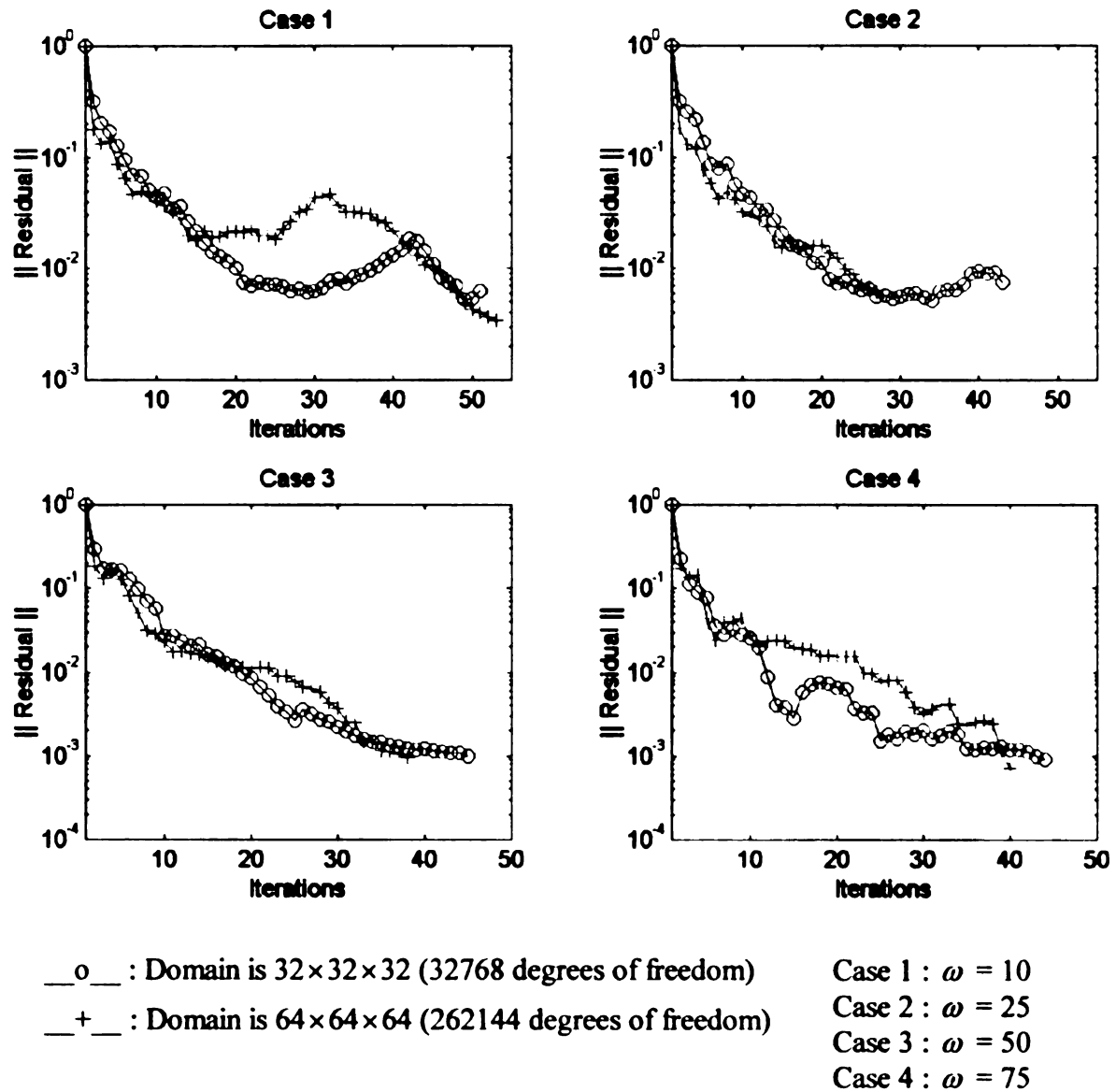


Figure 4.8 Performance of the solver for different frequencies and resolutions.

Figure 4.9 shows the frequency response plots obtained at the point of application of the force.

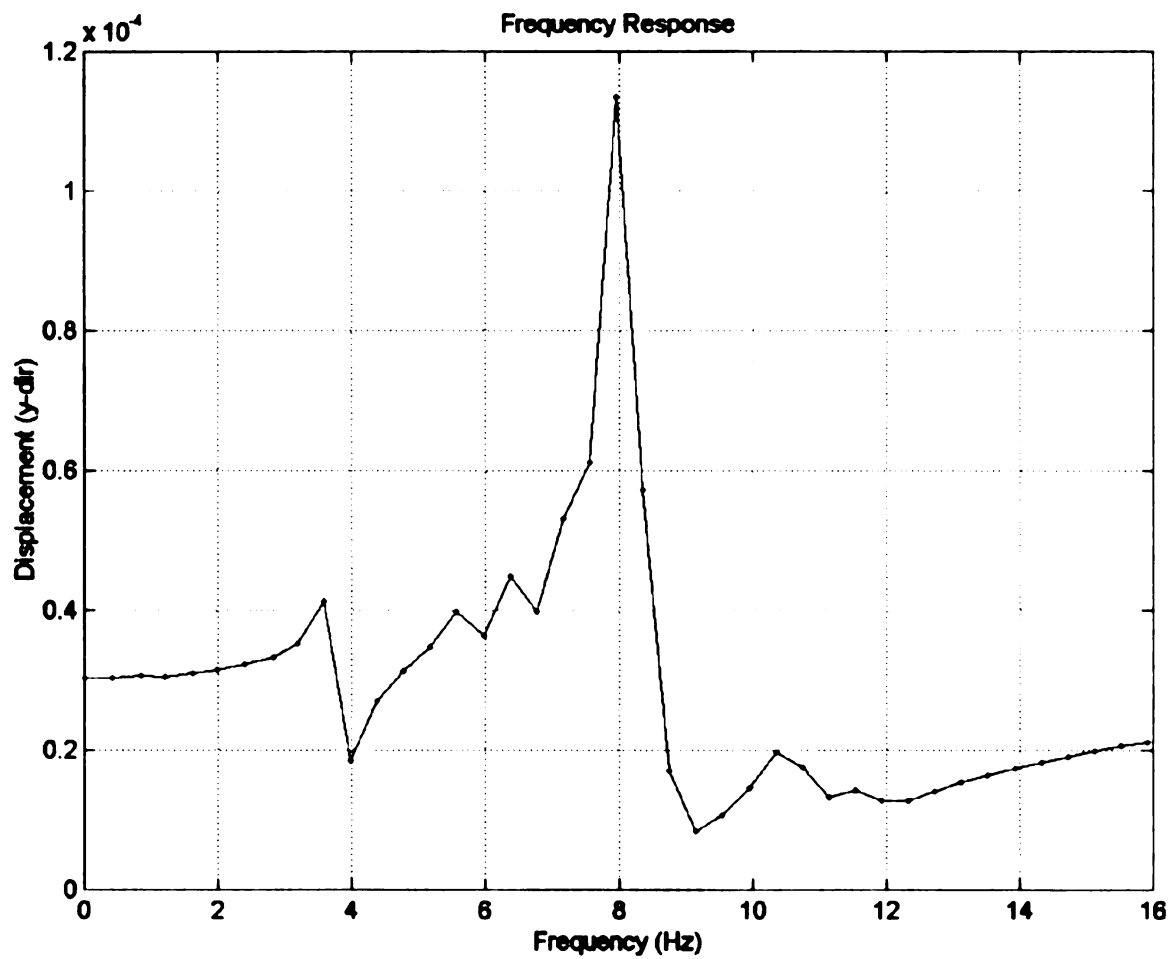


Figure 4.9 Frequency response plot at the point of application of the load.

Chapter 5

Conclusions

The standard finite element techniques have been successfully modified using a fictitious domain technique to solve frequency response problems in two and three dimensions.

Our initial goal was to develop a solution technique that would be significantly less computation and memory intensive than the standard finite element procedure.

The fictitious domain method has completely eliminated the time consuming meshing process. The convergence rate of our solver for different resolutions of the domain has been fairly insensitive to the size of the domain, which is a substantial improvement over the standard finite element procedure where the convergence rate decays as the size of the domain increases. The accuracy of the results obtained using the above fictitious domain technique have also

been shown to be on par with the results obtained using standard finite element schemes for the problems considered.

Areas of Future Work

- The inversion of the homogeneous coefficient matrix can be made still less computation intensive by using a better FFT algorithm.
- The sparseness of the various vectors and matrices used could be taken advantage of by storing only the non-zero entries, thus making the scheme a lot more memory efficient.
- For problems with large number of boundary conditions, the use of the Sherman-Morrison formula, which is computation intensive, could be avoided by using alternative strategies such as, PCG within a PCG approach to invert the preconditioner.

Appendix

The QMR from BCG Algorithm

This section presents the complete statement of the Quasi-Minimal-Residual from Bi-Conjugate Gradient algorithm, a solution method to solve the system of complex, symmetric linear equations $\hat{A} \mathbf{z} = \mathbf{F}$ using a slight variation of the method discussed in [13].

Preconditioned-QMR-from-BCG algorithm:

(0) Choose $\mathbf{z}_0 \in \mathbb{C}$

Compute the vectors

$$\mathbf{v}_1 = \mathbf{F} - \hat{\mathbf{A}} \mathbf{z}_0, \quad \mathbf{x}_1 = \mathbf{P}^{-1} \mathbf{v}_1 \quad \text{and} \quad \mathbf{p}_1 = \mathbf{x}_1$$

Compute the scalars

$$\tau_1 = \mathbf{x}_1^H \mathbf{v}_1, \quad \rho_1 = \mathbf{x}_1^T \mathbf{v}_1$$

Set $\mathbf{d}_0 = \mathbf{0} \in \mathbb{C}$ and $\mathcal{G}_0 = 0 \in \mathbb{C}$

For $n = 1, 2, \dots$ do :

(1) Compute the matrix-vector product

$$\mathbf{t}_n = \mathbf{A} \mathbf{p}_n$$

(2) Compute $\sigma_n = \mathbf{p}_n^T \mathbf{t}_n$

If $\sigma = 0$, then stop

(3) Set

$$\alpha_n = \frac{\rho_n}{\sigma_n} \text{ and } \mathbf{v}_{n+1} = \mathbf{v}_n - \mathbf{t}_n \alpha_n$$

(4) Compute the scalars

$$\mathcal{G}_n = \frac{\mathbf{x}_{n+1}^H \mathbf{v}_{n+1}}{\tau_n}, \psi_n = \frac{1}{1 + \mathcal{G}_n} \text{ and } \tau_{n+1} = \tau_n \cdot \mathcal{G}_n \cdot \psi_n$$

(5) Update the vectors

$$\begin{aligned} \mathbf{d}_n &= \mathbf{d}_{n-1} (\psi_n \mathcal{G}_{n-1}) + \mathbf{p}_n (\psi_n \alpha_n) \\ \mathbf{z}_n &= \mathbf{z}_{n-1} + \mathbf{d}_n \end{aligned}$$

(6) If \mathbf{z}_n has converged, then stop

(7) If $\rho_n = 0$, then stop.

(8) Set

$$\rho_{n+1} = \mathbf{x}_{n+1}^T \mathbf{v}_{n+1}, \beta_n = \frac{\rho_{n+1}}{\rho_n}$$

$$\mathbf{p}_{n+1} = \mathbf{x}_{n+1} + \mathbf{p}_n \beta_n$$

end.

Bibliography

- [1] J. Stephane, "Wavelet methods for fast resolution of elliptic problems", *SIAM J. Numer. Anal.*, 29, 965-986 (1992)
- [2] A. R. Diaz, "A wavelet-Galerkin scheme for analysis of large-scale problems on simple domains", *Int. J. Numer. Meth. Engng.*, 44, 1599-1616 (1999)
- [3] G. DeRose, A .R. Diaz, "Single scale wavelet approximations in layout optimization", *Structural Optimization* 18: (1) 1-11 (1999)
- [4] G. DeRose, "Solving topology optimization problems using wavelet-Galerkin techniques", *PhD Dissertation, Michigan State University, East Lansing, MI*, (1998)
- [5] J. H. Bramble and J. E. Pasciak, "A preconditioning technique for indefinite systems resulting from mixed approximations for elliptic problems", *Math. Comp.*, 50, 1-17 (1988)
- [6] R. O. Wells Jr. and X. Zhou, "Wavelet solutions for the Dirichlet problem", *Numerische Mathematik*, 70: (3) 379-396 (1995)
- [7] R. Glowinski, A. Rieder, R. O. Wells Jr. and X. Zhou, "A wavelet multi-grid preconditioner for Dirichlet boundary value problems in general domains", *RAIRO-Mathematical Modelling and Numerical Analysis*, 30: (6) 711-729 (1996)
- [8] R. Glowinski, T. W. Pan, R. O. Wells Jr. and X. Zhou, "Wavelet and finite element solutions for the Neumann problem using fictitious domains", *Journal of Computational Physics*, 126: (1) 40-51 (1996)
- [9] N. S. Bakhvalov and A. V. Knyazev, "Fictitious domain methods and computations of homogenized properties of composites with a periodic

- structure of essentially different components”, In G. I. Marchuk, editor, *Numerical Methods and Applications*, CRC Press, 221-266 (1994)
- [10] L. Meirovitch, “Principles and Techniques of Vibrations” Prentice Hall (1997)
 - [11] R. W. Freund, “Conjugate gradient-type methods for linear systems with complex symmetric coefficient matrices”, *SIAM Journal on scientific and statistical computing*, 13, 425-448 (1992)
 - [12] R. W. Freund, M. H. Gutknecht and N. M. Nachtigal, “An implementation of the look-ahead Lanczos algorithm for non-Hermitian matrices”, *SIAM Journal on scientific and statistical computing*, 14, 137-158 (1993)
 - [13] R. W. Freund and T. Szeto, “A transpose free quasi-minimal residue square algorithm for non-Hermitian linear systems”, in R. Vichnevetsky, D. Knight and G. Richter, editors, *Advances in Computer Methods for Partial Differential Equations VII*, IMACS, 258-264
 - [14] Y. Saad, “Iterative methods for sparse linear systems” PWS (1996)
 - [15] C. Chao, “A remark on symmetric circulant matrices”, *Linear Algebra and its Applications*, 103, 133-148 (1988)
 - [16] W. H. Press; B. P. Flannery, S. A. Teukolsky, and W. T. Vetterling, “Sherman-Morrison Formula.” In *Numerical Recipes The Art of Scientific Computing*, Cambridge, England: Cambridge University Press, 1989.

MICHIGAN STATE UNIVERSITY LIBRARIES



3 1293 02092 9554